AD-758 714

10.6-MICROMETER DETECTOR ARRAY

R. Lange, et al

AIL

Prepared for:

Office of Naval Research
Advanced Research Projects Agency

February 1973

DISTRIBUTED BY:

NTIS

National Technical Information Service
U. S. DEPARTMENT OF COMMERCE
5285 Port Royal Road, Springfield Va. 22151

10.6-MICROMETER DETECTOR ARRAY

AD 738714

Final Report
(1 April 1972 to 31 December 1972)

February 1973

by

R Lange, J. Wolczok, A. DiNardo, R. Augeri,
D. Yustein, and F. Pace

AIL Report 0123-F
Prepared Under Contract N00014-72-C-0446
Project Code 2E90K21

DDC
APR 18 1973
E

for

Office of Naval Research
Washington, D. C.

Sponsored by

Advanced Research Projects Agency
ARPA Order No. 1806, Amendment No. 2/02-09-72

by

AIL, a division of Cutler-Hammer
Deer Park, New York 11729

This document has been approved for public release and sale; its distribution is unlimited.

The views and conclusions contained in this document are those of the authors and should not be interpreted as necessarily representing the official policies, either expressed or implied, of the Advanced Research Projects Agency or the U. S. Government.

Reproduced by
NATIONAL TECHNICAL
INFORMATION SERVICE
U S Department of Commerce
Springfield VA 22151

UNCLASSIFIED
Security Classification

DOCUMENT CONTROL DATA - R & D

(Security classification of title, body of abstract and indexing annotation must be entered when the overall report is classified)

1. ORIGINATING ACTIVITY (Corporate author)
AIL, a division of Cutler-Hammer
Deer Park, New York 11729

2a. REPORT SECURITY CLASSIFICATION
Unclassified

2b. GROUP

3. REPORT TITLE
10.6-MICROMETER DETECTOR ARRAY

4. DESCRIPTIVE NOTES (Type of report and inclusive dates)
Final Report (1 April 1972 to 31 December 1972)

5. AUTHOR(S) (First name, middle initial, last name)
R. Lange, J. Wolczok, A. DiNardo, R. Angeri, D. Yustein, and F. Pace

6. REPORT DATE	7a. TOTAL NO. OF PAGES	7b. NO. OF REFS
February 1973	81	11

8a. CONTRACT OR GRANT NO.	9a. ORIGINATOR'S REPORT NUMBER(S)
N00014-72-C-0446	
b. PROJECT NO. ZE90K21	0123-F
c.	9b. OTHER REPORT NO(S) (Any other numbers that may be assigned this report)
d.	

10. DISTRIBUTION STATEMENT

11. SUPPLEMENTARY NOTES	12. SPONSORING MILITARY ACTIVITY
	Office of Naval Research Washington, D.C.

13. ABSTRACT

An initial design for a 10 × 10 element heterodyne array was developed using 77 K, 1500-MHz photodiodes. Five PV-HgCdTe 150-MHz photodiodes were then tested on a subassembly of a heterodyne matrix array structure with NEP's below 1.5×10^{-19} W/Hz measured out to 150 MHz.

A thermal analysis was performed for 77 and 4.2 K matrix arrays with 150 and 1500 MHz operation to determine the cooler requirement for each case and the effect of the thermal loading on photomixer performance. The cooler requirement for PV-HgCdTe was determined to be ≤2 mW per element and ≤200 mW for the Ge:Cu (Sb) photomixers.

A thermal mockup of the 77 K, 1500-MHz, 10 × 10 array was tested verifying the multi-cable thermal load analysis, the greater than 30-dB isolation between channels, and the greater than 24-hour operating time of the thermal mockup dewar.

Details of illustrations in this document may be better studied on microfiche

DD FORM 1 NOV 65 1473

UNCLASSIFIED
Security Classification

14 KEY WORDS	LINK A		LINK B		LINK C	
	ROLE	WT	ROLE	WT	ROLE	WT
Heterodyne Receivers						
Image Plane Dissection						
PV - HgCdTe Photomixers						
Heterodyne Matrix Arrays						
Wide Bandwidth						

10.6-MICROMETER DETECTOR ARRAY

Final Report
(1 April 1972 to 31 December 1972)

February 1973

by

R. Lange, J. Wolczok, A. DiNardo, R. Augeri,
D. Yustein, and F. Pace

AIL Report 0123-F
Prepared Under Contract N00014-72-C-0446
Project Code 2E90K21

Date of Contract:	1 April 1972
Expiration of Contract:	31 December 1972
Amount of Contract:	$113,211

for

Office of Naval Research
Washington, D. C.

Sponsored by

Advanced Research Projects Agency
ARPA Order No. 1806, Amendment No. 2/02-09-72

by

AIL, a division of Cutler-Hammer
Deer Park, New York 11729

The views and conclusions contained in this document are those of the authors and should not be interpreted as necessarily representing the official policies, either expressed or implied, of the Advanced Research Projects Agency or the U. S. Government.

ib-

TABLE OF CONTENTS

LIST OF ILLUSTRATIONS

I. INTRODUCTION

The feasibility of coherent arrays of high-performance multi-element heterodyne receivers using 4.2 K Ge:Cu photoconductors and CO_2 lasers has been demonstrated by AIL on two previous ARPA/ONR programs (contracts N00014-68-C-0273 and N00014-70-C-0407). The objective of the present program was to further extend the technology required to build large, high-speed, heterodyne, matrix array receivers using 77 K photodiodes for 10.6-μm laser radiation.

The contract called for the following:

- Examine high-density cabling techniques and test a breadboard for thermal and electrical characteristics
- Perform a thermal analysis for matrix arrays designed for 77 and 4.2 K, and 150 and 1500 MHz operation with 10 × 10 elements to determine the cooler requirements. Testing a thermal mockup of the 77 K, 1500-MHz, 10 × 10 array
- Initiate a design for a 10 × 10 element array assuming 77 K, 1500-MHz photodiodes. Parametric tradeoffs would be performed to determine size, weight, optical requirements, and thermal requirements
- Mount and test, in a subassembly matrix, four 150-MHz HgCdTe photodiodes
- Investigate image plane dissection techniques appropriate for matrix arrays of 100 elements or larger toward the goal of batch processing the image dissector

In the earlier work, copper-doped germanium photomixers were mounted in a two-dimensional array structure and cooled to 4.2 K. To achieve nearly quantum noise limited sensitivity in the photomixers, 200 mW of local oscillator (LO) and dc bias power were required (Section VI). This represents an internal heat load of 20 W for a 10 × 10 array of photomixers. In addition, the heat leak of 100 coaxial cables that connect the cooled photomixer to the room-temperature preamplifiers adds

another 3 W. This heat load of 23 W near 4.2 K represents a very significant cooling requirement with resultant high cost, size, weight, and cooler sophistication.

The recent development of PV-HgCdTe photomixers at 77 K with high-frequency response and much lower LO power requirements, makes the adaption of the array technique for use with these photomixers advantageous. The reduced cooling requirement of about 2 mW per photomixer or 200 mW for a 10 × 10 array makes the interconnecting coaxial cabling heat load of approximately 2 W the limiting requirement. This load of 2.2 W near 77 K does not present a problem since small aircraft-type coolers are available in the 80 K range with cooling capacities of up to 5 W.

This report covers the adaption of the heterodyne array principle to 77 K photomixers and discusses the following areas pertinent to the use of PV-HgCdTe photomixers:

- Uniformity of response of a five-element array of PV-HgCdTe photomixers with equal LO power, tested on a subassembly of the 1500 MHz, 77 K array design
- Thermal analysis of the array mount for 150 and 1500 MHz response photomixers
- Telescope design to match the optical requirements of the 10 × 10 PV-HgCdTe array

In addition to this, other techniques involved in the array design were further investigated and include:

- High-density cabling techniques aimed at low electrical crosstalk between elements, low thermal conductivity, and low electrical loss
- Image plane dissection techniques aimed at batch processing the microlenses for use with an array of 100 elements or larger
- Thermal analysis of 4.2 K arrays with either a 150 or 1500 MHz frequency response

II. EVALUATION OF PV-HgCdTe PHOTOMIXERS AS ARRAY ELEMENTS

To perform effectively, the elements in an array of detectors must have fairly well-matched characteristics. However, the imposition of tight uniformity specifications on detectors can decrease the manufacturer's yield to the point of making their cost prohibitively large. For this program, it was decided for economic reasons to approach this problem by setting only one extreme value for each key parameter and after testing make adjustments in the operating point of the photomixer to achieve nearly matched performance.

To test this approach, a subassembly of five HgCdTe photodiodes was constructed. These detectors were purchased without any uniformity specification, only the following characteristics were specified:

- Minimum quantum efficiency
- Minimum cutoff frequency
- Minimum reverse to forward resistance ratio
- Square photodiode geometry with maximum side dimensions specified

These photomixers were then measured extensively in the laboratory to determine their frequency response, heterodyne NEP, quantum efficiency, and cutoff frequency. Upon completion of the individual detector measurements, the photomixers were selectively biased and IF amplification chosen to match the mixing responsivities between mixer channels. With equal LO power applied, the responsivities as a function of frequency were measured to determine how well the photomixer channels could be matched in an array. These results are as follows.

A. PHOTOMIXER CHARACTERISTICS

The five PV-HgCdTe detectors were tested at 77 K and exhibited the characteristics shown in Table 1.

TABLE 1. PV-HgCdTe DETECTOR CHARACTERISTICS

	Mixer				
	A	B	C	D	E
Area cm^2	6.1×10^{-4}	6.75×10^{-4}	6.75×10^{-4}	7.8×10^{-4}	8.1×10^{-4}
Forward resistance (ohms)	16	7	15	9.0	9.5
Reverse resistance (ohms)	500 at -0.400 V bias	200 at -0.300 V bias	1500 at -0.400 V bias	260 at -0.400 V bias	800 at -0.500 V bias
Forward to reverse resistance ratio	0.032	0.035	0.01	0.035	0.012
D* cm $Hz^{1/2}/W$	8.7×10^9	6.1×10^9	1.37×10^{10}	1.3×10^{10}	2.1×10^{10}
λmax (μm)	11.9	12.05	10.5	10.2	10.5

The detector areas and front to reverse resistance ratios were well within the purchase specifications of 4×10^{-4} to 9×10^{-4} cm^2 for the sensitive area and less than 0.2 for the front to reverse resistance ratio. The current/voltage characteristic curves with no signal were measured and are shown in Figure 1. The forward and reverse slope resistances were extracted from these curves and it can be seen that the front to reverse resistance ratios were much less than 0.2, indicating that the diodes are of a high quality for HgCdTe detectors.

The D* for all the detectors was greater than 6.1×10^9 cm $Hz^{1/2}/W$ when measured at 10.6 μm. All of the detectors were long wavelength detectors with their peak sensitivities occurring between 10.2 and 12.1 μm.

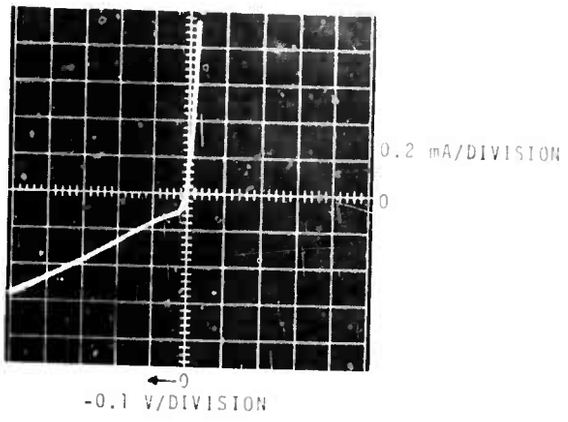

MIXER A

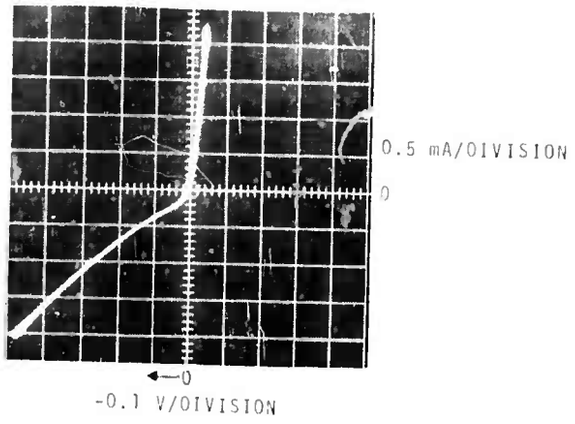

MIXER B

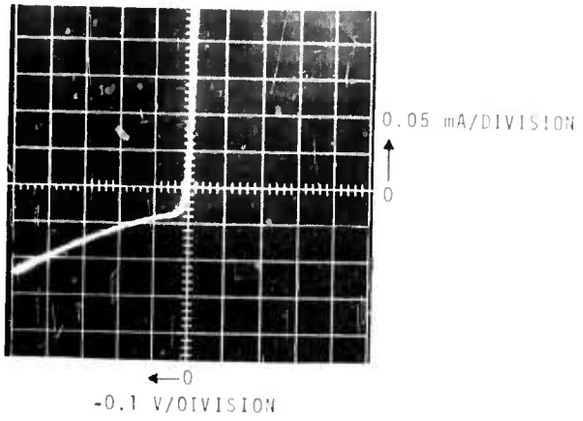

MIXER C

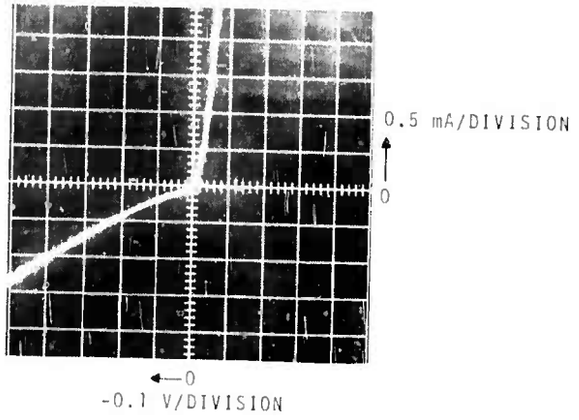

MIXER D

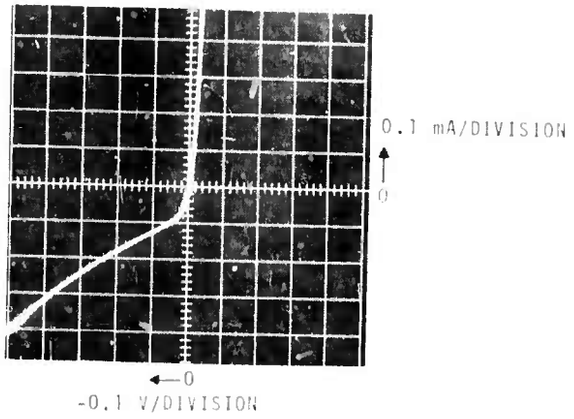

3-1093

MIXER E

FIGURE 1. VOLTAGE/CURRENT CHARACTERISTIC OF PV-HgCdTe PHOTODIODE

B. PHOTOMIXER FREQUENCY RESPONSE

Frequency response measurements were performed on the five photomixers using an indirect noise measurement technique (reference 1) in which the ratio of the thermal noise to the receiver noise (defined as the sum of thermal noise and shot noise) was measured. From the measured data, the ratio of shot noise to thermal noise for the receiver was calculated and is given in Figure 2 for the five photomixers. The mixer responsivity directly follows the shot noise to thermal noise curves because the IF signal power is directly proportional to the mixer shot noise power. From Figure 2 it can be seen that the mixer shot noise is approximately constant up to 100 MHz with all of the mixers exhibiting a 6 dB/octave rolloff, characteristic of an R-C limited photomixer. Mixer A is the one exception to the constant shot noise below 100 MHz, and the unusual behavior of mixer A can be attributed to an excess amount of 1/f noise which can be seen in Figure 3 to extend to about 70 MHz. Since the 1/f noise is greater than the thermal noise of the amplifier below 60 to 70 MHz, and is independent of LO power, it will lower the P_s/P_{th} ratio. This ratio decreases for increasing 1/f noise.

This, however, does not mean that mixer responsivity is decreasing from 20 to 60 MHz and must be disregarded when comparing the relative response of the mixers at low frequencies. An example of the typical 1/f noise behavior of acceptable detectors is shown in Figure 4 for mixer B where the 1/f noise falls below the level of the thermal noise at 70 kHz. This drastic difference in 1/f noise performance between detectors indicates that a 1/f noise performance specification should be imposed upon the detector when a large array is being implemented.

The cutoff frequencies for the particular bias points chosen in Figure 2 fall between 190 and 320 MHz where the cutoff frequency is defined by the intersection of the 6 dB/octave rolloff asymptote curve and the constant low frequency shot noise level. These cutoff frequencies were remeasured for several bias voltages for each mixer with the results shown in Figure 5. Using this dependence on bias voltage, the cutoff frequencies of the mixers can be adjusted to be equal for all mixer channels of an array. This is a powerful tool for improving the uniformity between mixer channels and is discussed further in paragraph D of this section.

C. MIXER SENSITIVITY

The heterodyne mixer noise equivalent power (NEP) was measured directly at 20 MHz for the array using two CO_2 lasers in a heterodyne setup with a fixed frequency offset of 20 MHz. Each mixer was illuminated

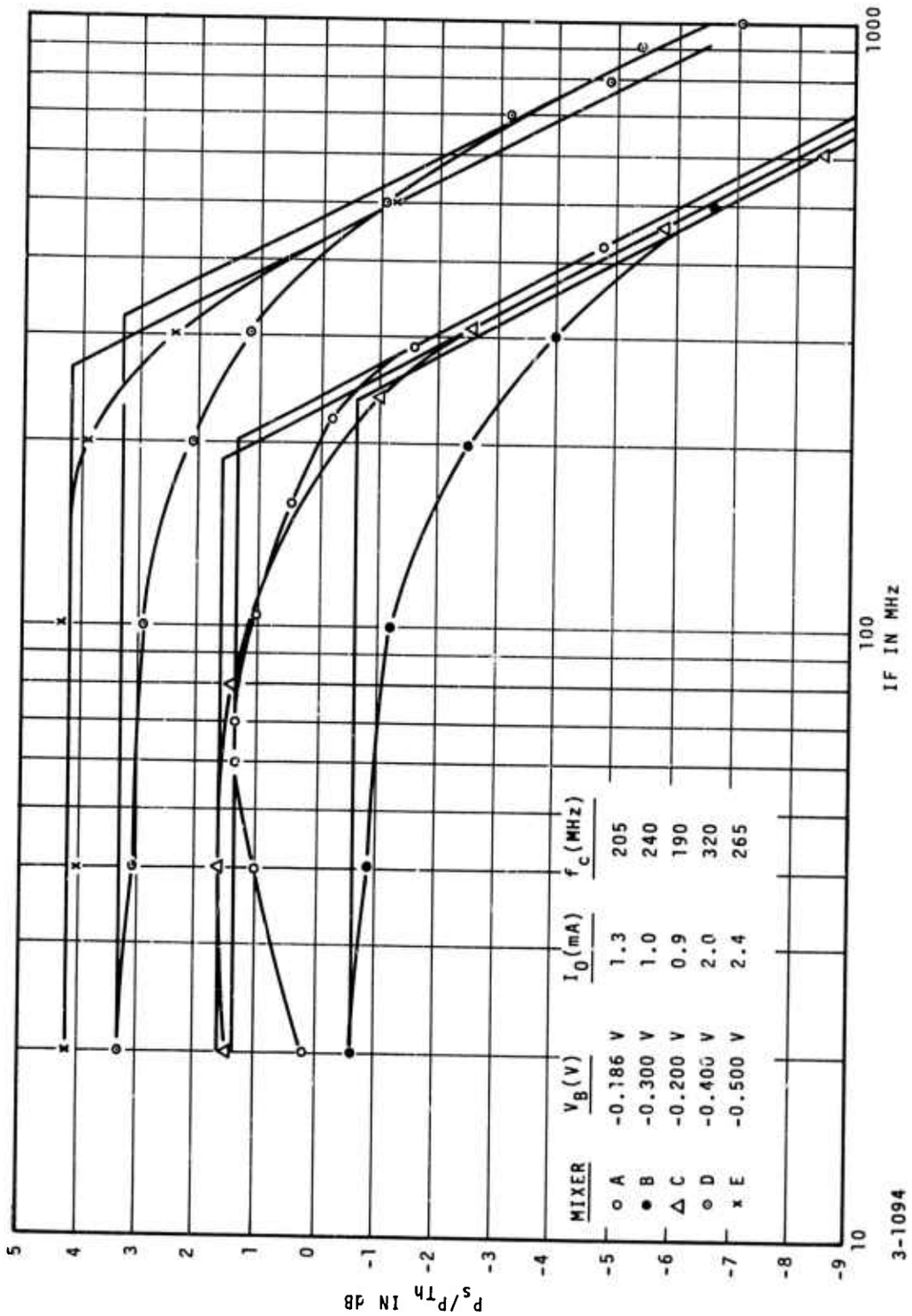

FIGURE 2. PHOTOMIXER SHOT TO THERMAL NOISE VERSUS FREQUENCY

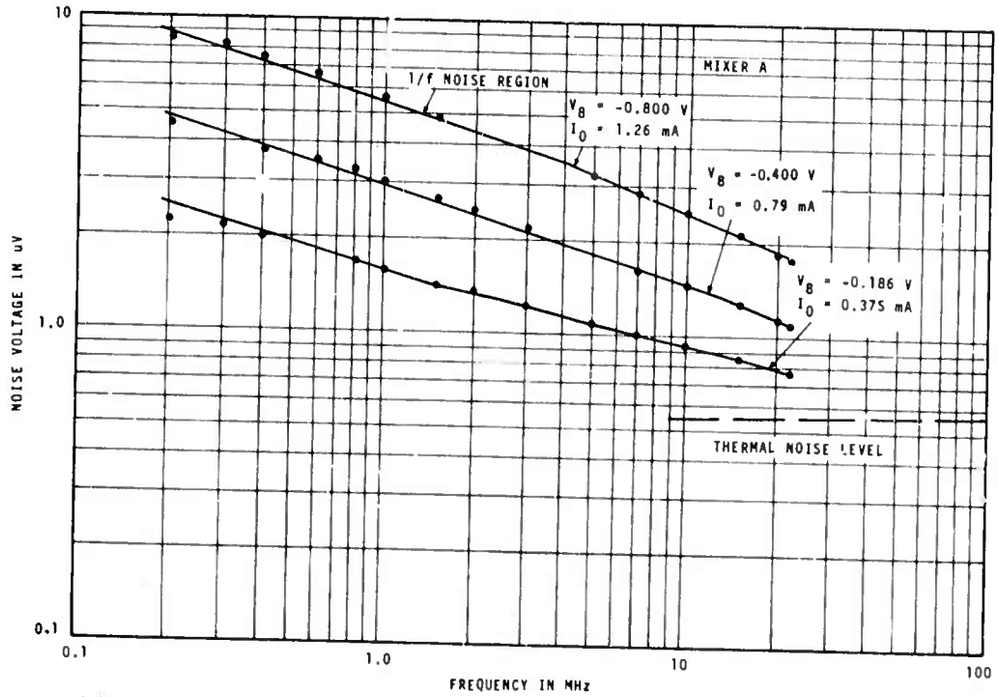

FIGURE 3. IF NOISE VERSUS FREQUENCY FOR MIXER A

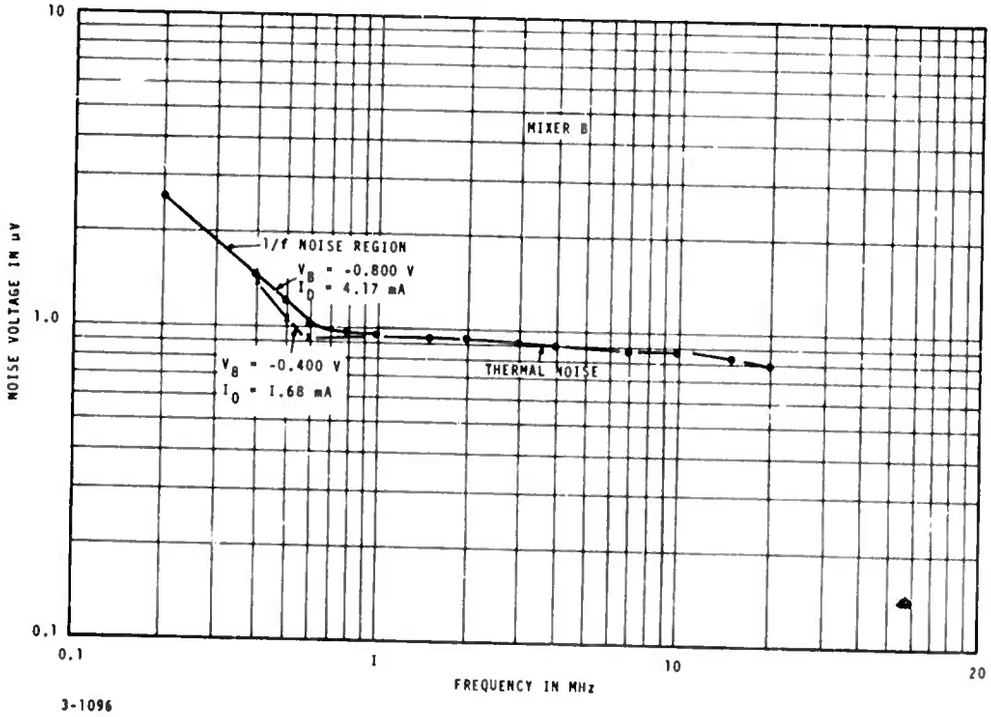

FIGURE 4. IF NOISE VERSUS FREQUENCY FOR MIXER B

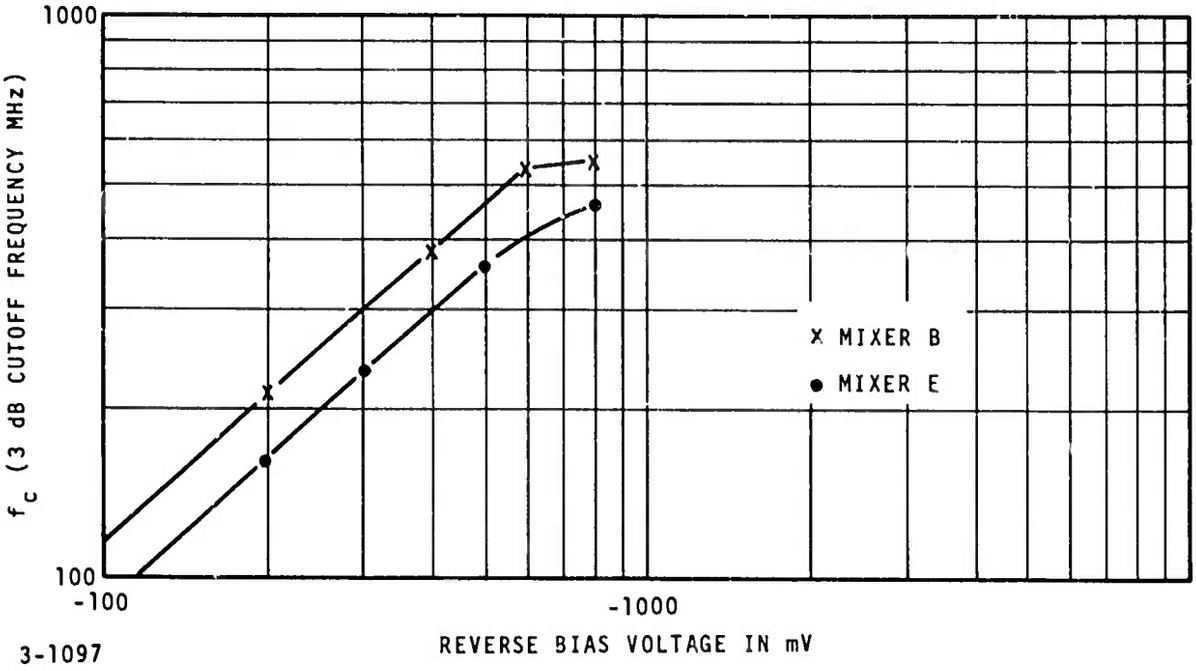

FIGURE 5. VARIATION OF CUTOFF FREQUENCY WITH BIAS VOLTAGE

by the same fixed amount of LO power computed from a fixed LO power density at the image plane dissecting lens array. The LO power used was approximately 0.5 mW per mixer element. Figure 6 gives the measured NEP values of the five detectors which range from 8.3×10^{-20} to 1.2×10^{-19} W/Hz. These values were obtained under the conditions indicated in Table 2 for the diode current, the photo-induced current, the shot to thermal noise, and the normalized sensitivity NEP/P_{min}. The IF amplifier used to evaluate the photomixers was extremely wideband, with a frequency response of 10 to 1500 MHz and a noise figure of approximately 5 dB. These values of NEP are then representative of a high-frequency response system to be used with Doppler offsets encountered with space vehicles. If the application is limited to aircraft with Doppler frequencies below 150 MHz, then a relatively narrowband amplifier would be used with a noise figure of about 2.5 dB and mixer NEP would more closely approach the quantum noise limited P_{min}.

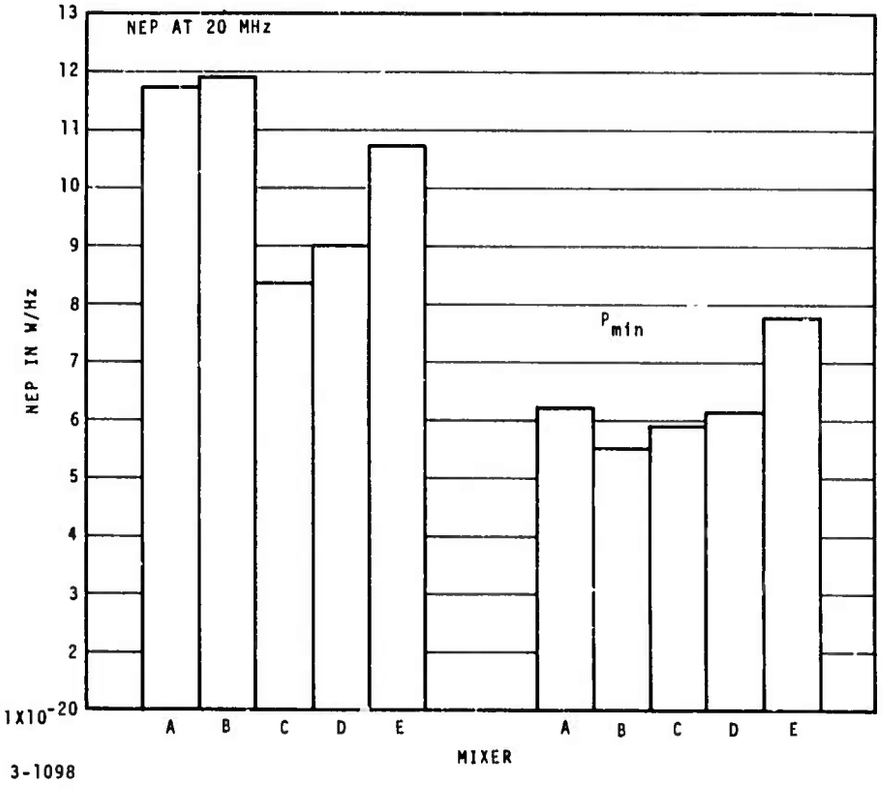

FIGURE 6. NEP AND P_{min} AT 20 MHz

TABLE 2. OPERATING CONDITIONS OF PHOTOMIXER ARRAY

		Mixer				
		A	B	C	D	E
P_s/P_{th}	(dB)	0.1	-0.7	1.4	3.3	4.2
NEP/P_{min}		1.96	2.16	1.71	1.46	1.38
I_{total}	(mA)	1.5	2.2	0.95	3.05	2.9
I_0	(mA)	1.3	1.0	0.85	2.0	2.4

From reference 2, the PV mixer design equations are used to determine P_{min} (quantum noise-limited NEP) and the quantum efficiency. Equation 1 allows determination of P_{min} based upon measurements of the NEP and the shot noise to thermal noise ratio.

$$NEP = P_{min} \left(1 + \frac{P_{th}}{P_{shot}}\right) \quad (1)$$

The results of this calculation of P_{min} are shown in Table 2 and vary from 5.5×10^{-20} to 7.9×10^{-20} W/Hz. From these values of P_{min}, we can then determine the small signal heterodyne quantum efficiency of the mixer from equation 2.

$$P_{min} = \frac{h\nu}{\eta} \quad (2)$$

where

h = Planck's constant

ν = frequency

η = quantum efficiency

The results of this calculation are shown in Table 3.

TABLE 3. SMALL SIGNAL HETERODYNE QUANTUM EFFICIENCY

Mixer	Quantum Efficiency (η) (Percent)
A	30
B	34
C	32
D	31
E	24

With the NEP at 20 MHz established, and the ratio of shot to thermal noise from 20 to 1000 MHz measured, the calculated NEP as a function of frequency based upon equation 1 can be plotted. This plot is shown in Figure 7 and it can be seen that the NEP's of all five mixers are below 1.4×10^{-19} W/Hz up to an IF of 150 MHz and below 3.0×10^{-19} W/Hz up to 500 MHz. These results are encouraging since the amplifier used was not optimized for the low frequency range of 10 to 150 MHz. Based upon these results, and the 2.5-dB noise figure of a 10 to 250 MHz preamplifier system, performance can be predicted for the optimized case. The calculated results are shown in Figure 8. From these curves it can be seen that the system NEP (that is, mixer/preamplifier combination) remains below 1.0×10^{-19} W/Hz over the desired 10 to 150 MHz bandwidth of an aircraft Doppler tracking or imaging system. The system, when used beyond this frequency range, only degrades 20 percent to 1.2×10^{-19} W/Hz at 250 MHz. This sensitivity is excellent for the specifications initially imposed on the mixers, and it is anticipated that a system with sensitivities of approximately 10^{-19} W/Hz could be built using the higher cutoff frequency photomixers that are available at the present time.

D. UNIFORMITY OF MIXER CHARACTERISTICS

The uniformity of response for five channels of the PV-HgCdTe photomixer array was determined from measurements of the mixer responsivity at 20 MHz and the mixer frequency response using a heterodyne measurement setup. The frequency response has already been described and is shown plotted in Figure 2. The mixing responsivity was measured at 20 MHz with an equal amount of LO power, 0.5 mW, on each mixer element, together with a high signal-to-noise ratio (SNR) between 67 and 70 dB. The mixed signal and noise are shown in Table 2.

The signal incident upon each mixer element was a plane wave with uniform flux density. The mixed signal response was therefore corrected for differences in the mixer sensitive areas as shown in Figure 9. The highest response mixer, E, was chosen as the reference channel and additional gain at IF was provided to the other channels to equalize the mixer channel responsivities before further processing. The additional gain required ranges from 3.9 dB for mixer B to 0.3 dB for mixer D. This gain was also applied to the noise, resulting in a 1.8-dB variation between channels. If the system using these detectors included a threshold detector, the overall sensitivity would be degraded by the varying levels of shot noise plus thermal noise among the channels. However, this tradeoff

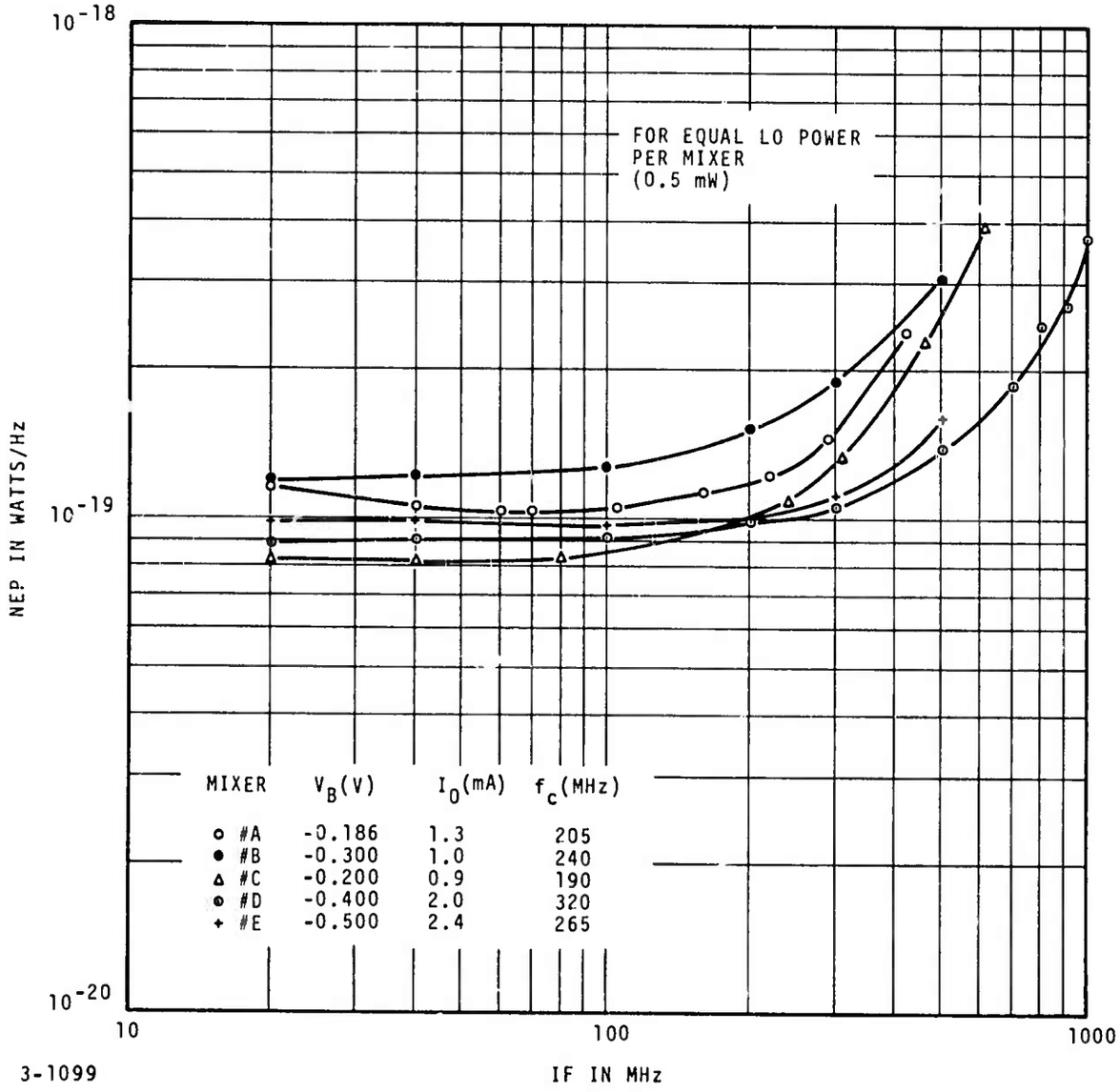

FIGURE 7. ARRAY NEP VERSUS FREQUENCY FOR WIDEBAND 10 TO 1500 MHz MIXER PREAMPLIFIER COMBINATION

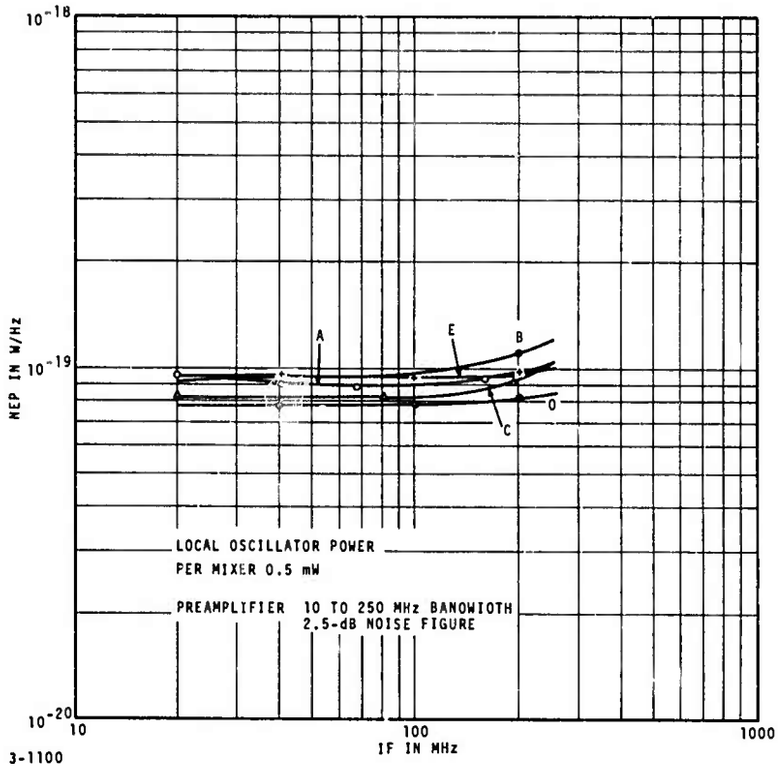

FIGURE 8. PREDICTED SYSTEM NEP FOR A 10 TO 250 MHz SYSTEM

resulted in matching the mixer channel responsivities as closely as shown in Figure 10, which data are derived from the data in Figure 2 by adjusting the gain per channel necessary to provide equal mixer channel responsivities at 20 MHz. All of the mixer responsivities follow those shown in Figure 2, with the exception of mixer A which had excessive 1/f noise.

From these curves the variation in response between channels is seen to be ±0.3 dB from 10 to 150 MHz for the best four mixers.

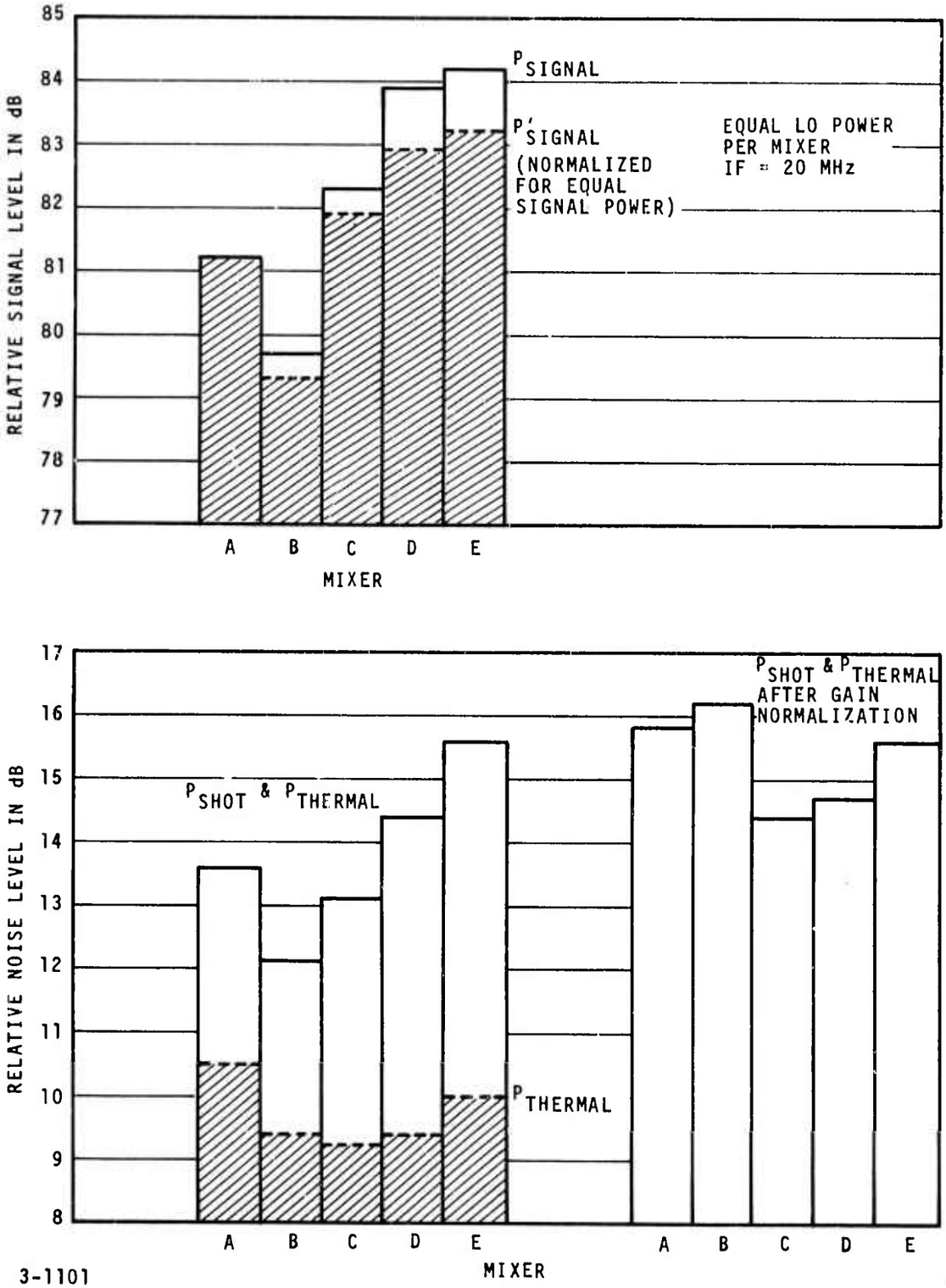

FIGURE 9. SIGNAL AND NOISE MEASURED AT 20 MHz

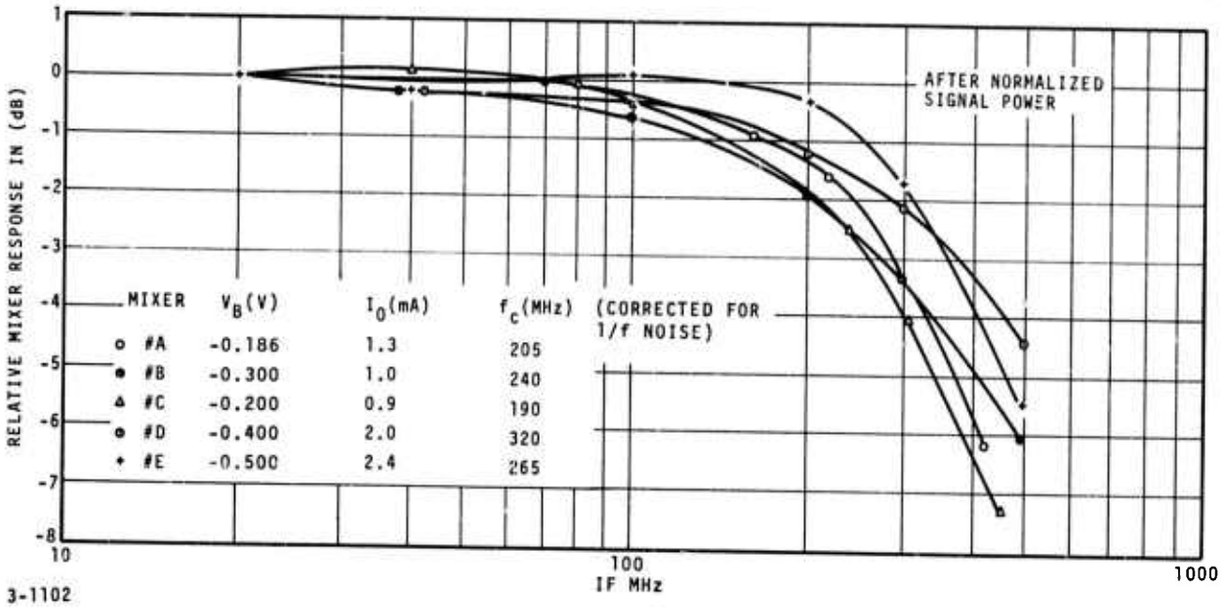

FIGURE 10. UNIFORMITY OF RESPONSE FOR FIVE PV-HgCdTe PHOTODETECTORS

This uniformity of response between channels is excellent and can be attributed to several factors:

- Mixer responsivities can be matched using varying IF gain between channels
- PV-HgCdTe is an R-C limited device exhibiting a characteristically flat low frequency response with a 6-dB octave rolloff beyond the cutoff frequency
- The mixer cutoff frequency is a function of the mixer bias voltage which varies the junction capacitance

The only limitation to more closely matching the mixer channels is their behavior in the neighborhood of the cutoff frequency. Some mixers exhibit a sharp rolloff between the flat and 6 dB/octave region such as mixer E, while others such as mixer D exhibit a more gradual transition in this region.

E. COOLING REQUIREMENT FOR PV-HgCdTe PHOTOMIXERS

For the most efficient operation of PV-HgCdTe photomixers they must be cooled to about 100 K as seen in reference 2. To maintain the mixers at this temperature, the cooler must handle the power absorbed from both the infrared LO and the dc bias source. The LO and dc bias power requirements are deduced from the measurements in the preceding sections for 10 to 150 MHz operation and from the mixer design equations presented in Appendix A.

1. LASER LO POWER REQUIREMENTS

The LO power level is set by the bandwidth requirements of the system. From Appendix A it can be seen that between 0.5 and 2.0 mW per mixer element are required for near quantum noise-limited performance of 10^{-19} W/Hz. Operation at 10 to 150 MHz requires 0.5 mW, and 2.0 mW is needed for the full 10 to 1500 MHz bandwidth. The data presented in paragraph C of this section support these results for 10 to 150 MHz operation where NEP's of 10^{-19} W/Hz were obtained for a LO power of 0.5 mW.

2. DC BIAS POWER REQUIREMENTS

The dc bias power dissipated in the mixer is due to the diode leakage current and the current photo-induced by the LO. The leakage current of present high-speed photodiodes with high reverse resistance may be 10 to 20 percent as large as the photo-induced current when the diodes are biased below the current breakdown region and LO powers on the order of 0.5 to 2 mW are used. For a first-order calculation of the heat load imposed by a HgCdTe photodiode on a cooler, the dc bias power can be neglected since its major component comes from the LO power which is converted to electrons in the photodiode.

Therefore, for 10 to 1500 MHz heterodyne operation, the total power dissipation will be 2 mW per mixer element for near quantum noise-limited operation at 10.6 μm.

F. THERMAL ANALYSIS OF PHOTOMIXER ARRAY MOUNTS

1. DETERMINATION OF THE TEMPERATURE RISE OF A PV-HgCdTe MIXER MOUNTED IN A 10 × 10 ARRAY

The temperature of the detector (Figure 11) is calculated for the steady state case by starting with the thermal resistances between the

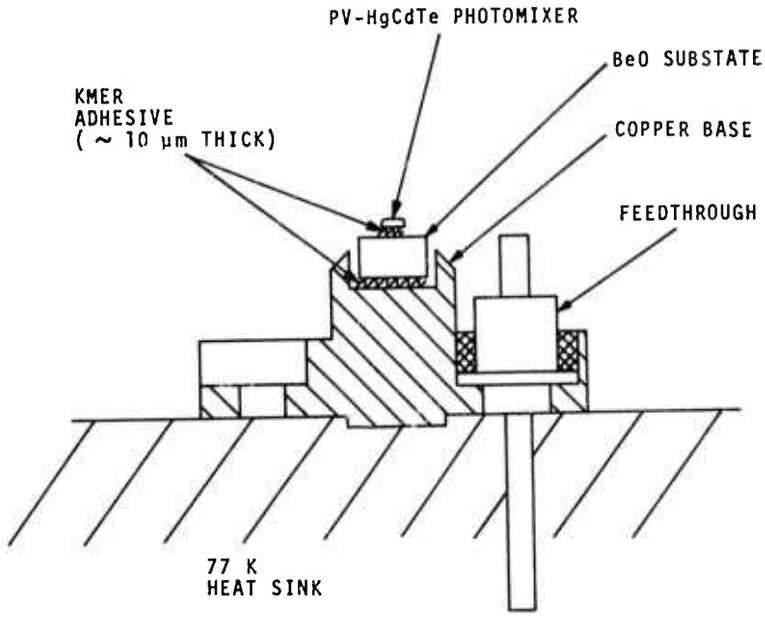

FIGURE 11. DETECTOR MOUNT FOR 77 K PV-HgCdTe PHOTOMIXER

mixer with its LO and dc bias power loads and the 77 K liquid nitrogen cold sink. From Fourier's expression for heat conduction, the thermal resistance of a material is determined by the distance the heat must travel through the material divided by the cross-sectional area times a constant for the material (thermal conductivity). The thermal resistances for the various portions of the heat sink are 0.55 K/W for the BeO substrate, 1/3 K/W for the Cu, and 25 K/W for the KMER adhesive between the mixer, substrate, and Cu base. The temperature difference between mixer and cold sink is obtained from equation 3:

$$\Delta T = \sum Q R_{Th} \qquad (3)$$

For an assumed 2 mW of input heat load due to the incident laser LO and thermal resistance of 26.8 K/W, a ΔT or temperature rise of 0.054 K above the heat sink can be anticipated for the fully illuminated PV-HgCdTe mixer operating at 77 K. As a result of this very small temperature rise of the photomixer, we can conclude that there will be no deterioration of the sensitivities of the central mixer elements of a 77 K PV-HgCdTe photomixer matrix array.

III. IMAGING ARRAY AND ASSOCIATED OPTICS

A. TELESCOPE DESIGN FOR 77 K PV-HgCdTe PHOTOMIXER ARRAY

An optical system has been conceived which permits the construction of a 10 × 10 array of HgCdTe photovoltaic mixers with a frequency response of up to 1.5 GHz. The features of the design include:

- Ability of the array to be made up of individually mounted detector elements allowing implementation of the array concept with any number of detectors to prove feasibility, optimum choice of the array elements for a matched or more uniform response from the array, and allows replacement of damaged elements
- Low optical and electrical crosstalk between channels due to the relatively large spacing between detectors and the separate coaxial cable outputs

The optical approach chosen is shown in Figure 12 and is an extension of that which was developed under ONR Contract N00014-68-C-0273. The optical system is basically the same because an image is subdivided by an array of square lenses directing all the optical energy from one cell in the focal plane to the appropriate infrared mixer element. However, the HgCdTe photovoltaic detectors require a relatively large spacing between detectors to provide for mounting and cabling, and to ensure low electrical and optical crosstalk.

Because of this large spacing requirement, a matching lens was added to match the diffraction-limited spot in the primary focal plane of the telescope to a square image-dissection lens in the secondary focal plane. This matching lens effectively increases the f/number of the primary receiving optics to provide a diffraction limited disc that matches the image-dissection array. In this way, mixer center-to-center spacings of 7.5 mm (which would otherwise correspond to a telescope f/number of 300) can be achieved with a lower f/number requirement on the receiving optics.

In this configuration, the LO is injected into the system between the matching lens and the image-dissection array. At the plane of the image-dissection array, the LO and signal are effectively plane waves with matched phase fronts. These two matched fields are then focused onto and mixed in the detector elements.

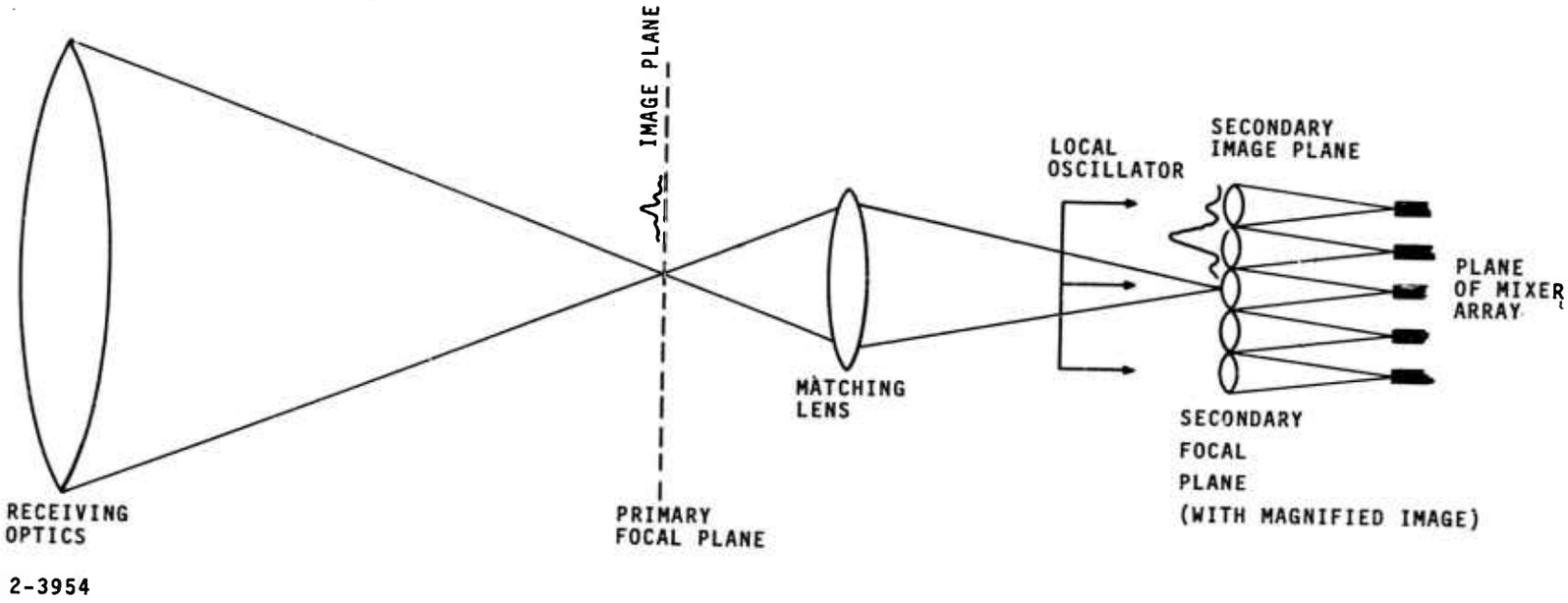

FIGURE 12. OPTICAL DIAGRAM OF IMAGING ARRAY

B. ARRAY PATTERNS FOR TELESCOPE WITH 77 K PV-HgCdTe PHOTOMIXER ARRAY

To analyze the behavior of the optical design presented in the previous section, it was necessary to mathematically formulate the optical train and obtain the field patterns of the LO and signal that were mixed and detected in the focal plane of the image-dissection array. The mathematical formulation was programmed on a digital computer to give design information for optimizing the array patterns. The optical efficiencies and adjacent pattern crossovers were obtained in this way.

From the array pattern synthesis found in Appendix B, we get:

$$I_m = C\left[\operatorname{Sin}(\omega - \omega_o)\, t\right] \cdot e^{ik/t_2\ (\bar{x}x + \bar{y}y)} \cdot$$

$$\frac{J_1\left\{\frac{k_a}{f_1}\left[(\underline{x} + \underline{x}_1)^2 + (\underline{y} + \underline{y}_1)^2\right]^{1/2}\right\}}{\frac{k_a}{f_1}\left[(\underline{x} + \underline{x}_1)^2 + (\underline{y} + \underline{y}_1)^2\right]^{1/2}} \cdot e^{ik/f_2\ (\bar{x}x + \bar{y}y)} \cdot dx\,dy\,d\bar{x}\,d\bar{y}$$

which gives the IF signal output from a mixer element located in the focal plane of the microlens image-dissection array. This integral was computed to give the far-field patterns for several combinations of LO and signal fields. Three-dimensional plots of the mixed signal output over the detector surface were also computed for several angles of arrival of the signal with respect to one of the image-dissection lenses.

Figure 13 shows the value of I_m which represents the product of the LO and signal field, evaluated at 100 points across the surface of the mixer element. Each of the 100-unit areas was treated as a separate mixer and the integral I_m was evaluated at each unit element, with their sum representing the IF signal output of the mixer.

The parameters initially chosen were an f/400 telescope, a square (1.1 × 1.1 cm) image-dissection lens f/3.8, and a plane wave LO incident upon the image-dissection lens. The f/400 telescope approximately matches the diffraction-limited spot from the telescope, to the square image-dissection lens rejecting most of the out-of-phase side-lobe energy for the on-axis case. Figure 14 shows both the signal and LO fields focused on the

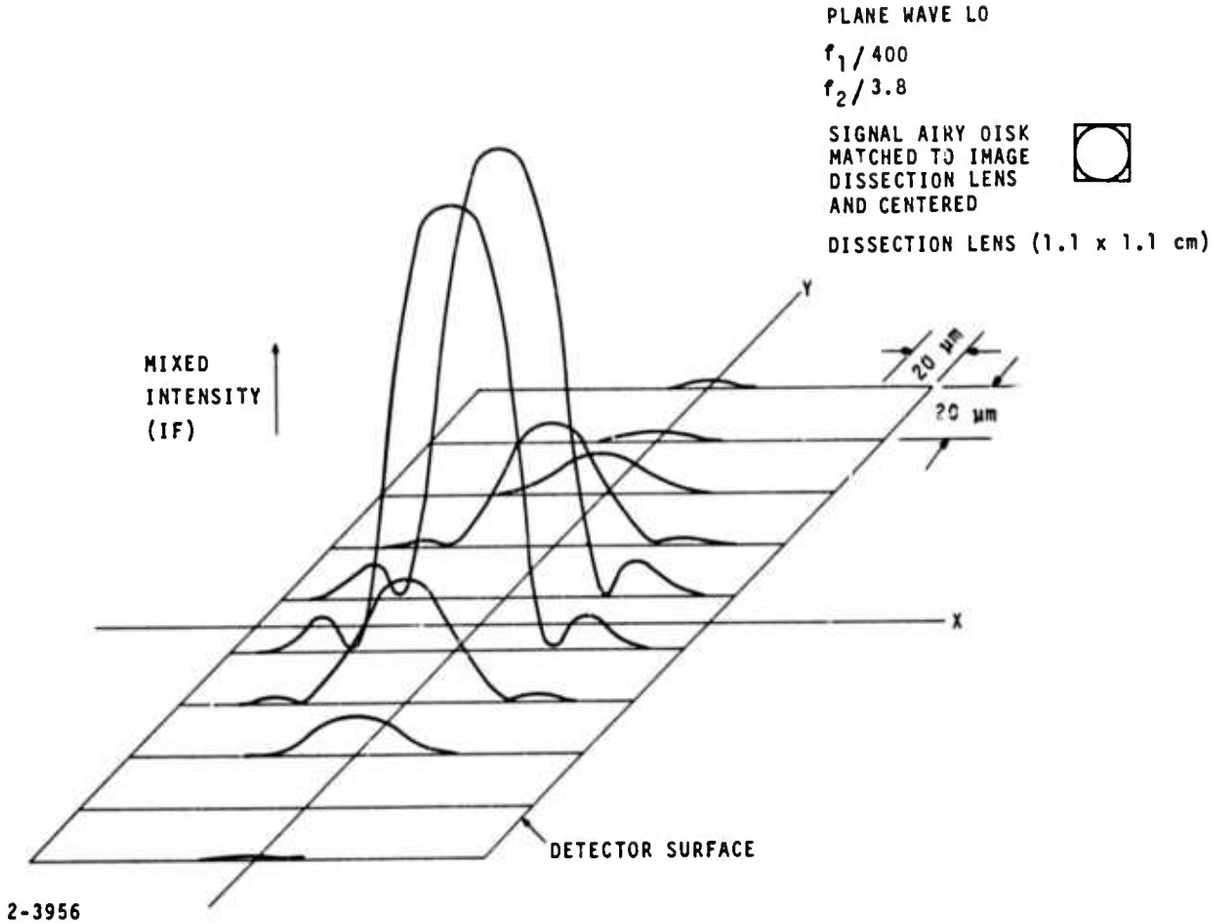

FIGURE 13. MIXER INTENSITY AT DETECTOR SURFACE FOR PLANE WAVE LO, $f_1/400$ AND SIGNAL CENTERED

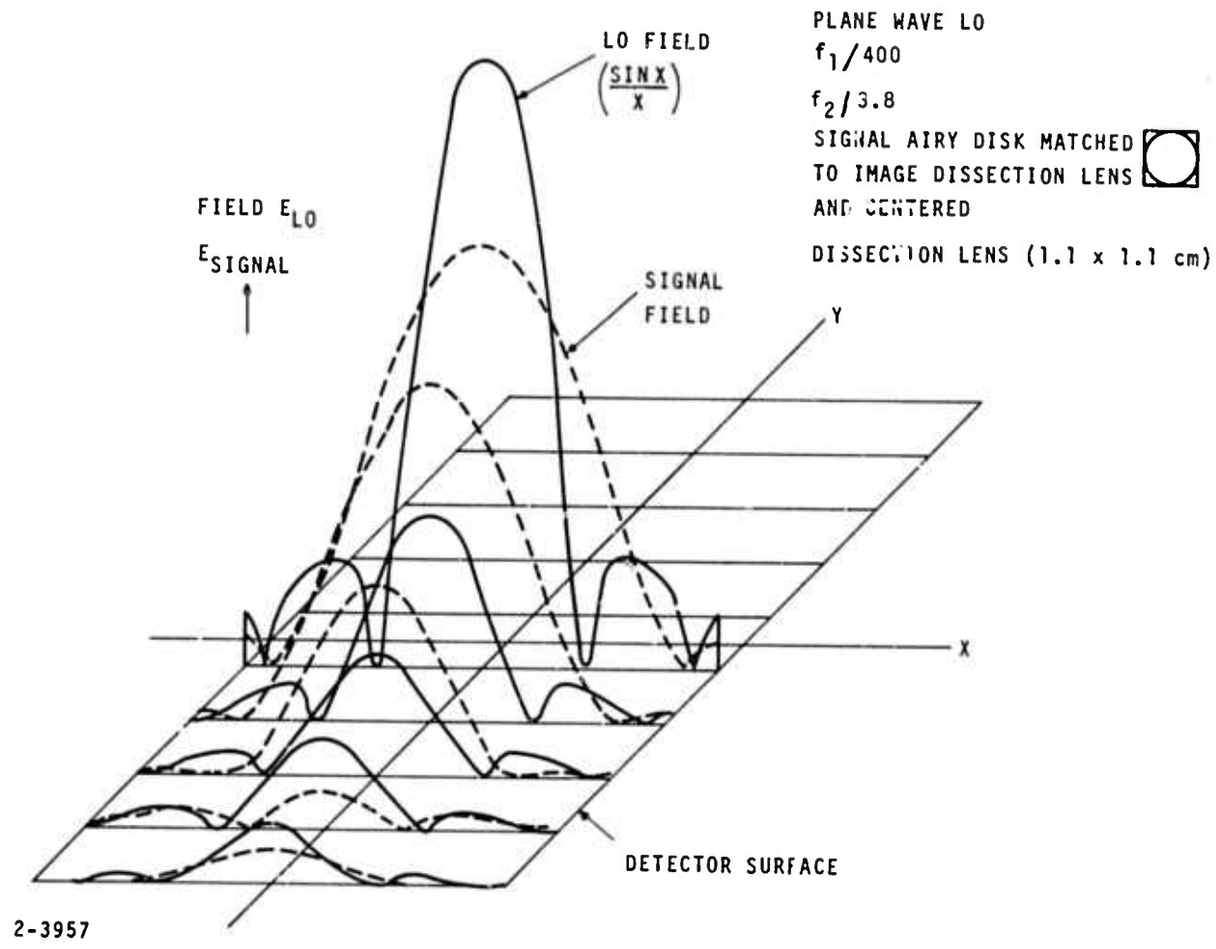

FIGURE 14. LO AND SIGNAL FIELD AT DETECTOR SURFACE

mixer. It can be seen that at the mixer, the signal field $[J_1(x)/x]$ approximately matches the size of the detector while the LO field $(\sin x/x)$ is considerably narrower. This difference in the diameters of the signal and LO spots is due to the different amplitude distributions across the image-dissection lenses. With the signal spot centered on an image-dissection lens, there is little or no energy at the edges of the lens and its effect at the detector is to produce a higher effective f/number. Since the LO gives a uniform intensity distribution across the image-dissection lens aperture, and the diffraction limited spot size depends directly on f/number, a signal spot larger than that of the LO is obtained.

This combination of parameters introduces an inefficiency in that the phases of the signal and LO are not matched across the surface of the mixer. Over the area of the LO airy disc, the signal and LO are both in phase and contribute to the IF signal output. The first side lobe of the LO also falls upon the detector surface but it is 180 degrees out of phase with the central field of the signal. The result is that the product of the two fields in this region is negative and subtracts from the IF signal output degrading overall receiver sensitivity. This degradation can be reduced by reducing the size of the detector or increasing the image-dissection lens f/number. The detector can then be matched to the size of the mixer airy disc rejecting most of the out-of-phase mixer signal.

To determine the crossover levels between elements of the array, the signal airy disc was positioned at the edge of the image-dissection lens with half of the airy disc energy falling on a single image-dissection lens. Figure 15 shows the mixed signal across the mixer face for this case with the same f/numbers and plane wave LO as Figure 13. If the detector was reduced in size to more effectively match the on-axis case, it would reduce the sensitivity at the crossover point. The reason for this is that the second ring of the diffraction pattern beyond the airy disc will no longer fall upon the mixer. This ring is in phase with the central field and has a significant amplitude. Therefore, a rejection of this ring loses signal power causing a loss of sensitivity.

The second case to be examined has the same signal conditions $f_1/400$, $f_2/3.8$, and image-dissection lens $(1.1 \times 1.1$ cm), but the local oscillator field across the image lens was changed as follows. An amplitude taper was applied to the LO making it similar to the Gaussian shaped signal field. This has the effect of matching the focused fields of the LO and signal over the mixer surface such that the energy in the airy disc and the side lobes is additive to the IF signal. For this case it is advantageous to collect all of the IF signal energy by increasing the mixer size. Figures 16 and 17 show the mixed field across the mixer surface for the on-axis and edge case. It

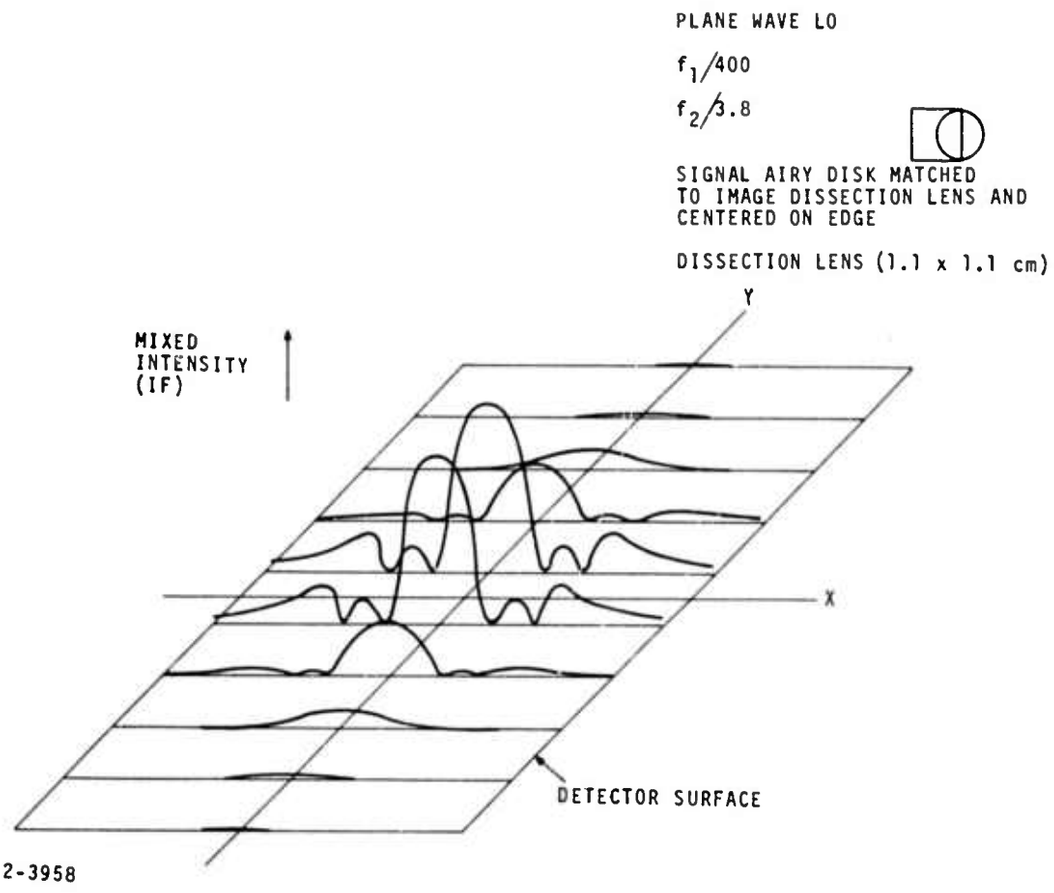

FIGURE 15. MIXER INTENSITY AT DETECTOR SURFACE FOR PLANE WAVE LO, $f_1/400$ AND SIGNAL CENTERED ON EDGE

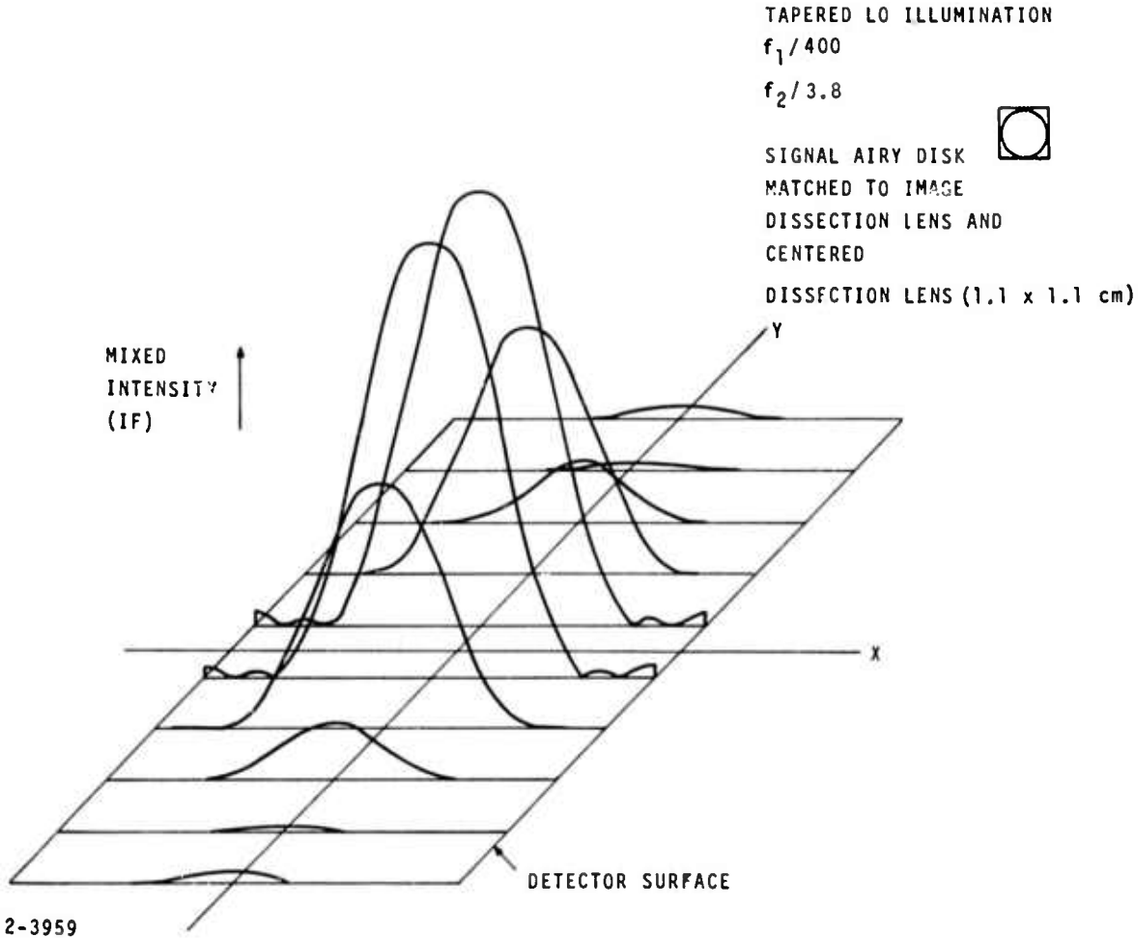

FIGURE 16. MIXER INTENSITY AT DETECTOR SURFACE FOR TAPERED LO, $f_1/400$ AND SIGNAL CENTERED

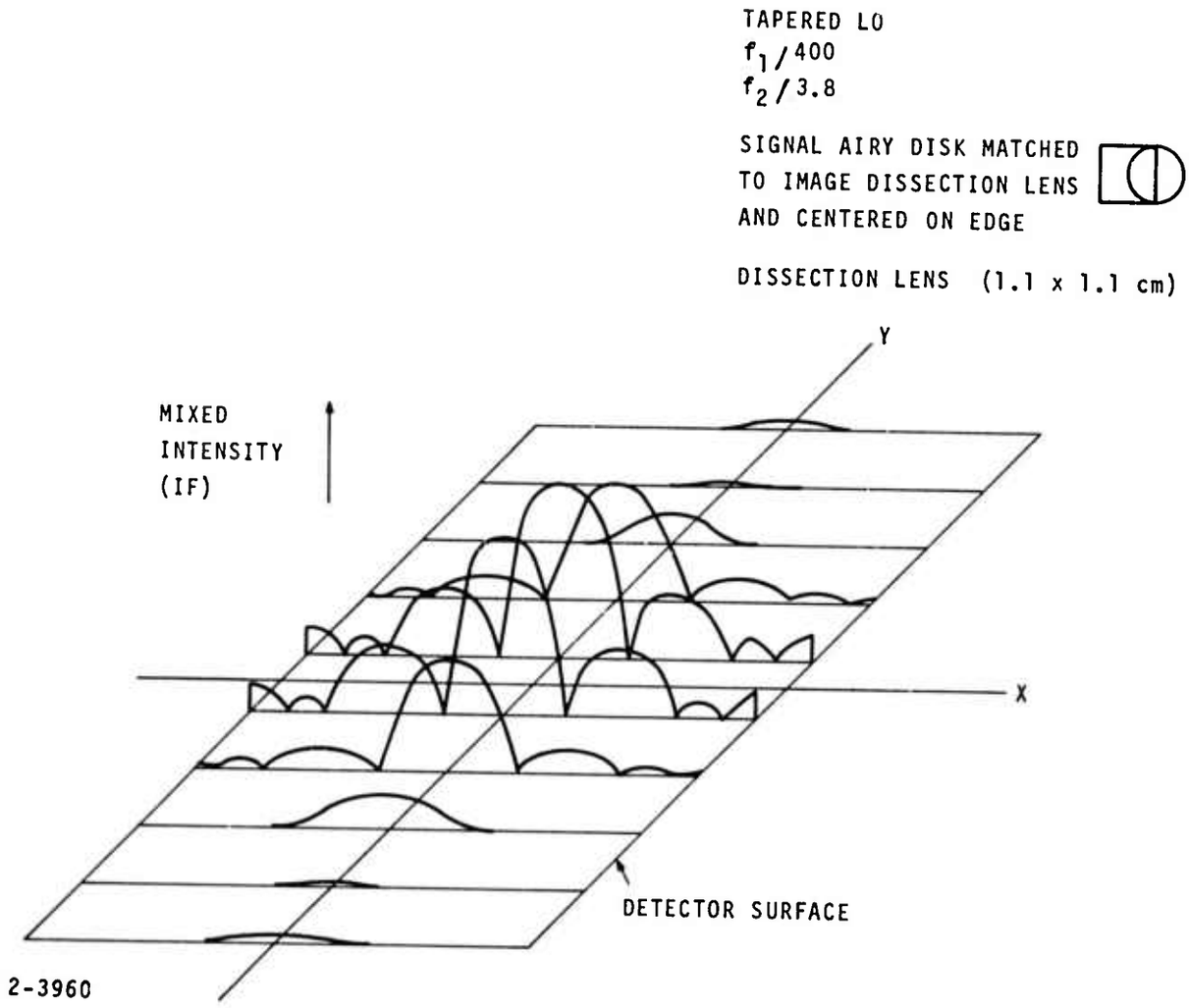

FIGURE 17. MIXER INTENSITY AT DETECTOR SURFACE FOR TAPERED LO, $f_1/400$ AND SIGNAL CENTERED ON EDGE

can be seen that the IF signal airy disc is now larger and better matches the detector size.

The third case is for a plane wave LO, with all parameters the same as the first case except for a larger f/number telescope ($f_1/800$). This case is closer to that of a coherent heterodyne monopulse receiver where the signal airy disc is matched in size to a 2 × 2 square array of image-dissection lenses. This case has higher crossover levels and it is anticipated that this will not be an effective configuration for obtaining the best image resolution for a fixed number of array elements. It is, however, another instructive case which shows a closer match of the LO and signal field across the detector with little out-of-phase IF contribution. This case has been measured in the laboratory and data are shown in Figure 2-11 of reference 3. This data agrees very closely with Figures 18, 19, and 20, and also shows very clean mixed IF patterns in the focal plane of an image-dissection lens array even with the signal airy disc centered on the edge of a dissection lens.

The far-field patterns for the three cases are plotted in Figure 21. This plot shows the integrated mixer outputs versus a normalized array element spacing. The crossovers are:

LO	Telescope f/number	Edge Crossover (dB)	Corner Crossover (dB)
Plane wave	400	- 4.3	8.1
Plane wave	800	- 2.2	-4.8
Tapered	400	-10.7	--

Since the mixer center to center spacing of 11 mm was reduced to approximately 8.0 mm during this program, we can reduce the telescope f/number required to produce the crossovers shown above with the resulting crossovers for the system described as follows:

LO	Telescope f/number	Edge Crossover (dB)	Corner Crossover (dB)
Plane wave	300	- 4.3	-8.1
Tapered	300	-10.7	--

From this correspondence between the telescope f/number and the crossover level, the optimum optical system can be obtained for use with a given array element spacing. This optimum crossover level, however, must still be

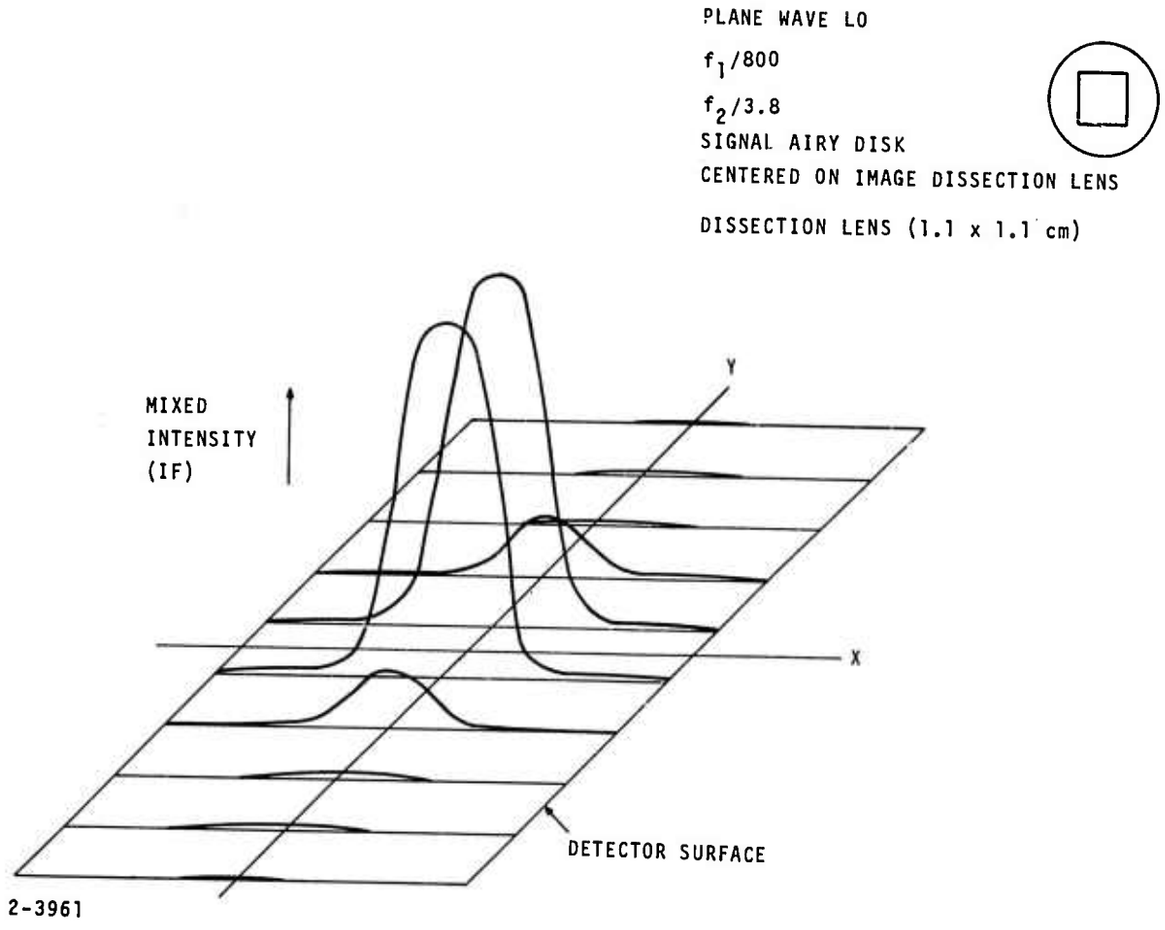

FIGURE 18. MIXER INTENSITY AT DETECTOR SURFACE FOR PLANE WAVE LO, $f_1/800$ AND SIGNAL CENTERED

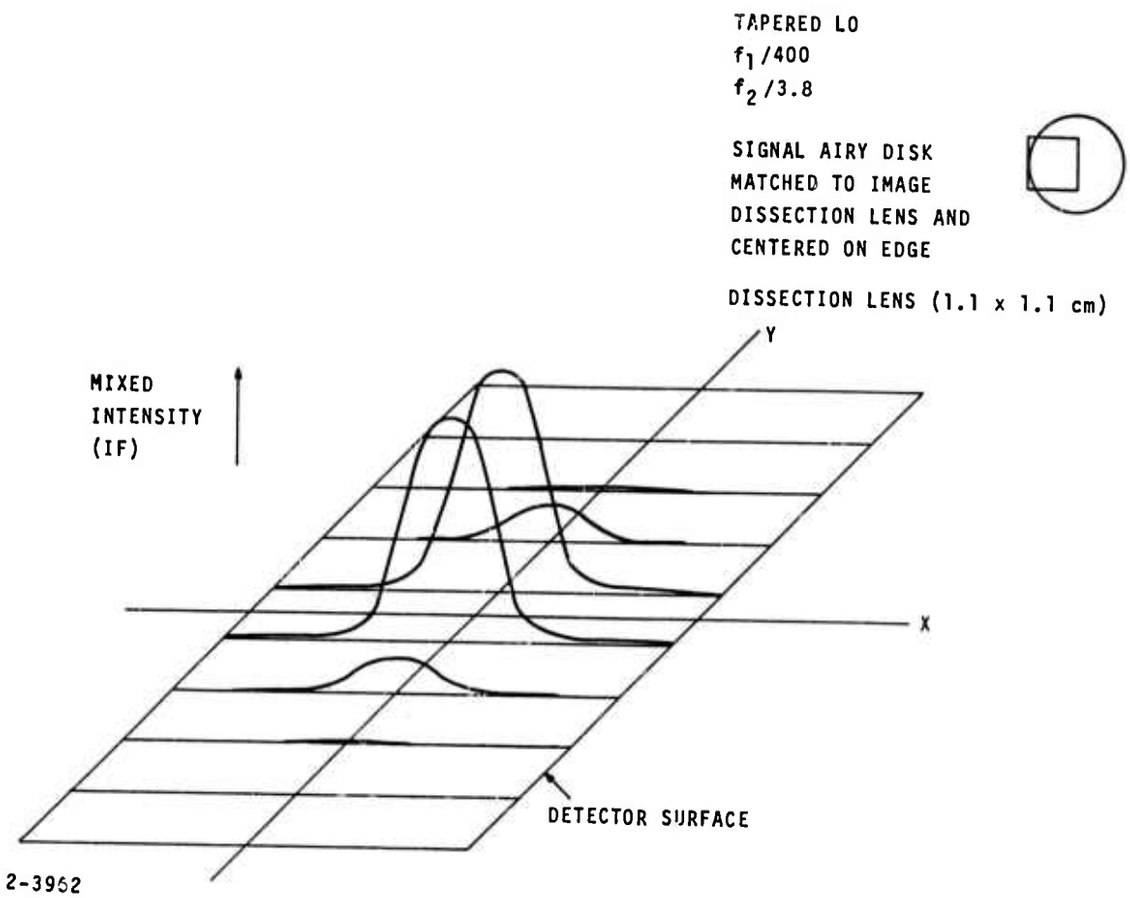

FIGURE 19. MIXER INTENSITY AT DETECTOR SURFACE FOR PLANE WAVE LO, $f_1/800$ AND SIGNAL CENTERED ON EDGE

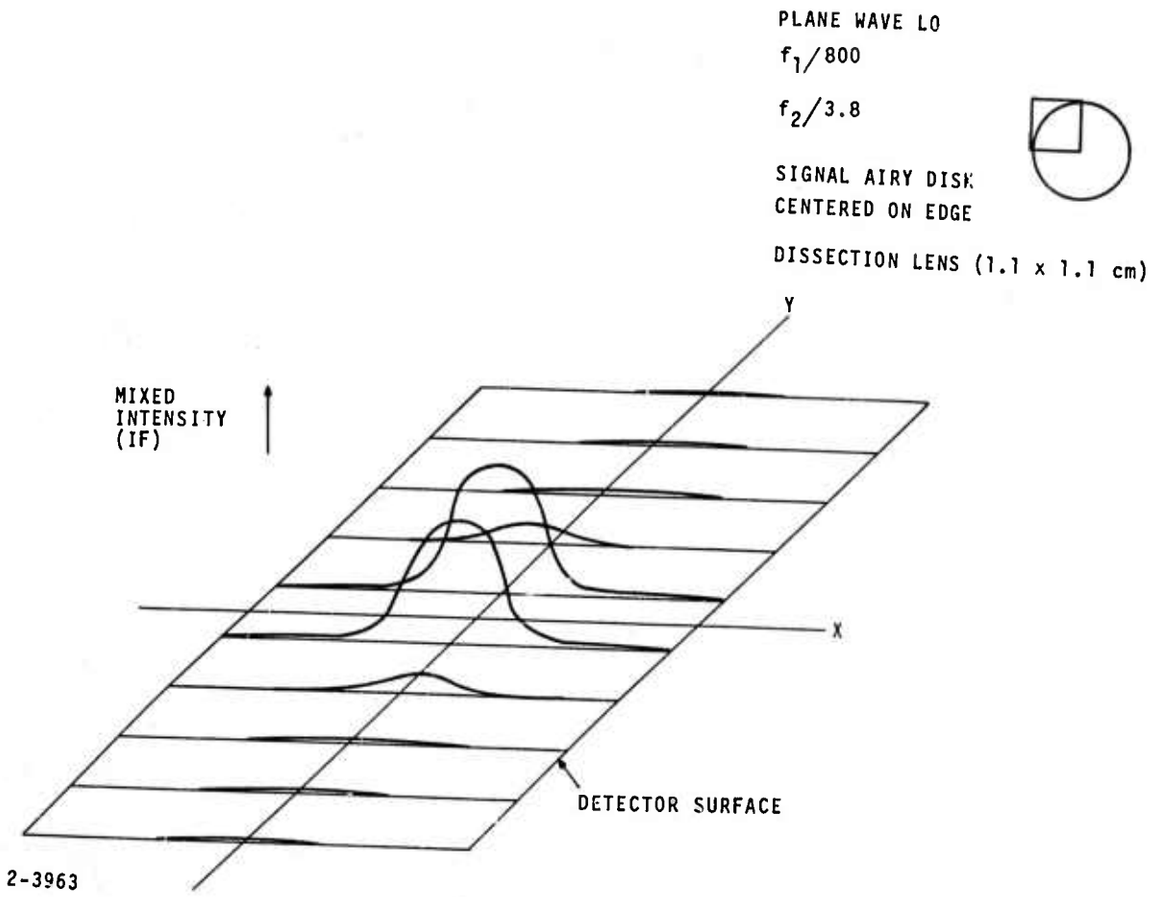

FIGURE 20. MIXED INTENSITY AT DETECTOR SURFACE FOR PLANE WAVE LO, $f_1/800$ AND SIGNAL CENTERED ON EDGE CORNER

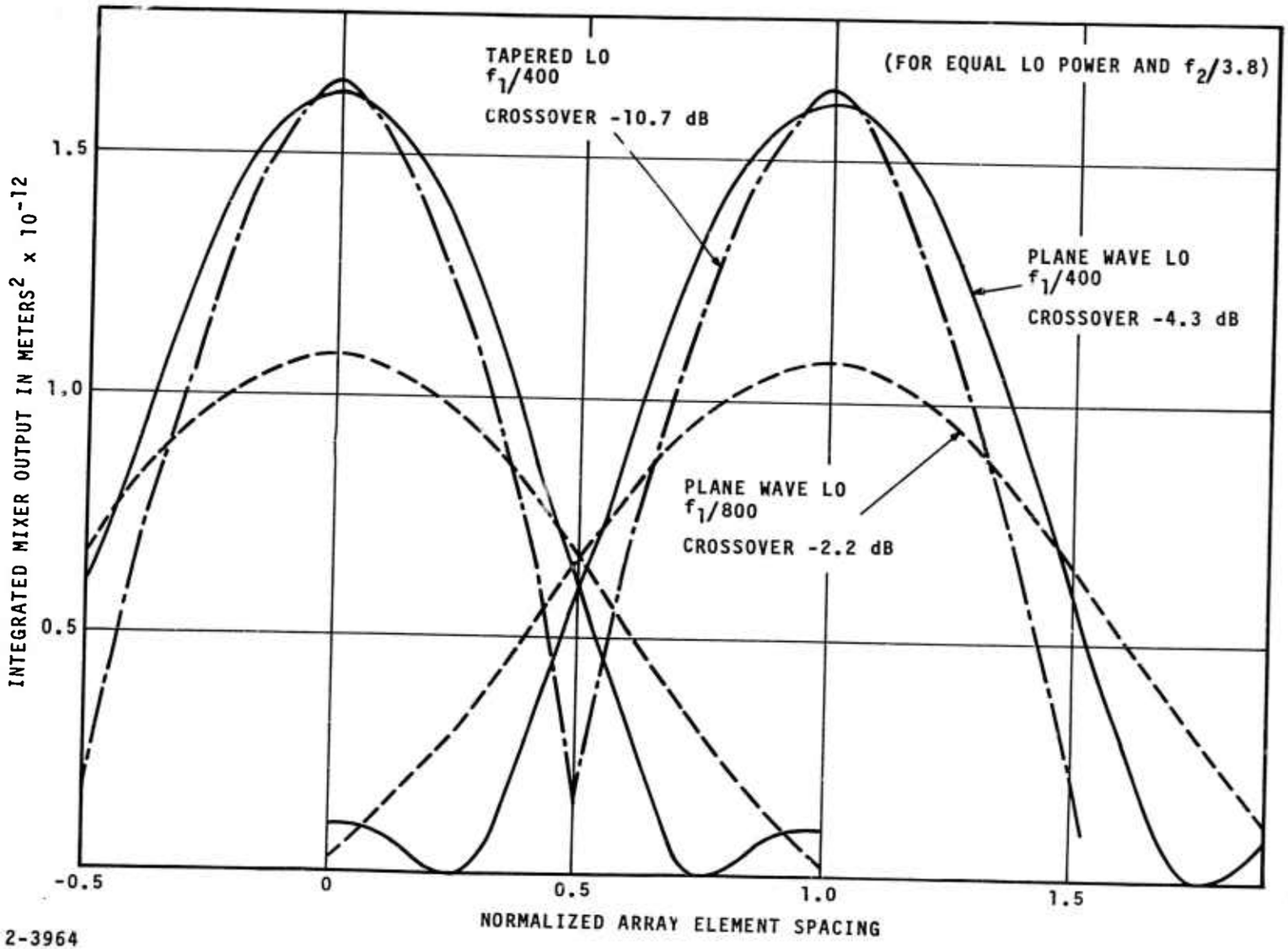

FIGURE 21. FAR-FIELD ARRAY PATTERN FOR CONFIGURATIONS OF LO AND SIGNAL ILLUMINATIONS

obtained from a study of image quality for a finite number of individual resolution cells. For the purposes of proceeding with this program, this can be conducted on a future program, since the only change needed to re-optimize would be the telescope f/number.

C. IMAGE PLANE DISSECTION TECHNIQUES

Image plane dissection techniques were investigated toward the goal of batch processing the elements for arrays of 100 elements or larger. Five techniques were studied, with preliminary fabrication and testing being conducted where possible within the scope of the present program. The five approaches are:

- Fresnel lens array prepared by a cold forming technique
- Molding of GeSbSe IR transmitting glass
- Fresnel zone plate arrays
- Batch processing of germanium lenses
- Photolithographic fabrication of thin-film lens arrays.

1. FRESNEL LENS ARRAY

A Fresnel lens was constructed for use at 10 μm to test the feasibility of cold-forming techniques. Previous technology in this area has been confined to the visible and near infrared due to a lack of suitable materials transmitting in the infrared at 10.6 μm. A material (silver bromide) has been identified which appears likely to fit the needs of the array transmission at 10.6 μm. The material has the ability to cold flow which is necessary for the fabrication technique employed, however, it is photosensitive, changing its transmission if exposed to ultraviolet light for extended periods of time. This does not present a restriction to the array application since the lenses will be located in a dewar flask behind a germanium window. The Ge does not pass the ultraviolet so that no deterioration of the lens is likely to result.

Tests were performed to evaluate the lens for the application of image dissecting for the 10 × 10 array program. This lens was illuminated with collimated radiation at 10.6 μm for various aperture sizes. The primary focal length at the operational wavelength was found to be 3/8 inch. The intensity distribution at the focal plane (Figure 22) was obtained by scanning an 0.008 inch, square detector across the plane. It can be observed from the figure that as the f/number increases (aperture diameter decreases), the spot size decreases. This occurrence indicates operation far removed

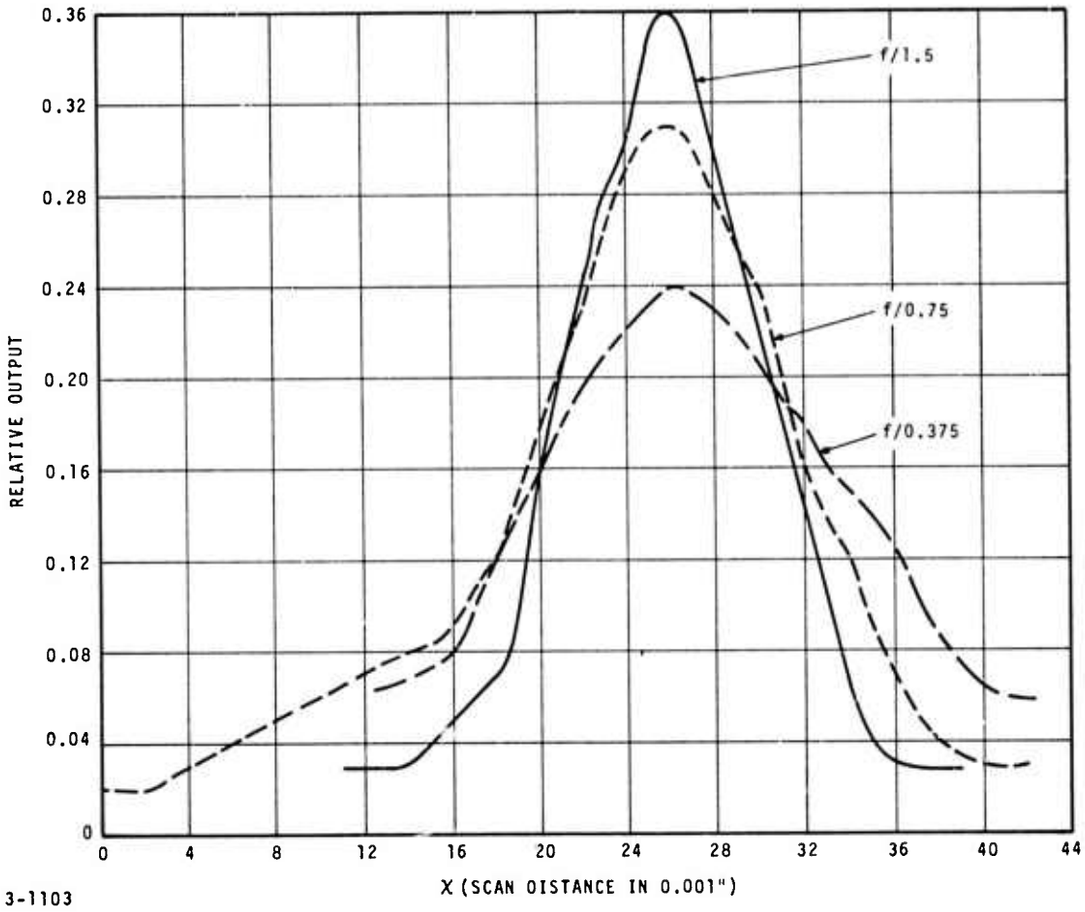

FIGURE 22. DISTRIBUTION AT FOCAL POINT OF FRESNEL LENS

from the diffraction limit performance required. For the f/1.5 case approximately 70 percent of the energy in the focused spot falls on the 0.008 inch, square detector. The ratio of the detector output with and without the Fresnel lens in front of it was measured to be $\frac{E_2}{E_1} = 199$. In the ideal case this ratio of energy collected for the two optical schemes is the ratio of the areas intercepting the collimated beam. This computes to an optical gain of 766. Taking the ratio of the measured value and dividing by the ideal case value, a measure of the efficiency of the lens is obtained

$$\text{Efficiency} = \frac{199}{766} = 0.26$$

This 26 percent efficiency indicates that most of the radiation is diffracted into other orders or scattered by the lens and for this reason it is presently not suitable for the application at hand. More development work would be required in this area to raise its performance to acceptable levels.

2. MOLDING OF INFRARED GLASS

The molding of a GeSbSe glass array has been investigated and appears to be feasible. However, no lens array was fabricated due to the unavailability of a suitable source presently having sufficient experience in molding this glass. The scope of the present program is such that a subcontract to explore this technique is not called for at this time.

The material's transmission is 65 percent (1 to 11 μm) with virtually all of the loss due to reflection and minimum material absorption up to 11 μm (reference 4). Antireflection coatings are available which increase the transmission in the 8 to 11 μm band to better than 90 percent. This material has been readily formed into various shapes by melt-casting with high quality lenses resulting. Consultations with the glass manufacturers indicate that the molding of a multiple lens array as a single unit is feasible and the tolerances will be set by the master mold which can be very precisely controlled.

3. FRESNEL ZONE PLATE ARRAYS

Fresnel zone plate arrays can also be used for the image-dissection technique with fabrication techniques well within the state of the art. They, however, have the disadvantage of a high optical loss of the signal energy (3 dB) due to reflection of the energy from alternate out-of-phase zones. It is felt that this loss cannot be tolerated in a high sensitivity receiver.

4. BATCH PROCESSING OF Ge LENSES

The batch processing of individual square germanium lenses can be accomplished with sufficient tolerances to ensure a minimum buildup of dimensional tolerances across the array. However, the area of potential difficulty in using this approach is the control of the center-to-center spacing of the focused spots in the focal plane. Any cocking of the lens or shift in optical axis from the lens center will shift the position of the focused spot off the desired optical axes of the array.

5. PHOTOLITHOGRAPHIC FABRICATION OF LENSES

Photolithographic techniques for the fabrication of a thin film lens array have come about as a result of the utilization of integrated circuit technology. The lens profile is approximated by an N-step phase quantization with the layers formed by successive photoengravings using N masks (reference 5). Experimental results by d'Auria and others show a 63 percent diffraction of the incident energy into the main focus of the lens for a four-level lens as compared with the theoretical 81 percent. This resultant 63 percent efficiency is judged to be below that already feasible using several of the techniques described previously.

Based upon the data available to this point, we must conclude that the relatively low efficiency yielded by the Fresnel zone plate arrays and the photolithographic thin-film lenses make them impractical for a near-quantum noise-limited array.

IV. HIGH-DENSITY CABLING TECHNIQUES FOR WIDEBAND MULTIELEMENT ARRAYS

High-density cabling techniques were investigated in order to determine the thermal load, electrical loss, and crosstalk for two types of cables which might be suitable for connecting the cryogenically cooled photomixers and the ambient temperature IF preamplifiers. Tests were conducted wherever practical to check the analytical results. The analysis was done for a 50-ohm twin lead cable and a 50-ohm semirigid coaxial cable. The twin-lead cable consisted of stainless steel conductors 0.010 inch in diameter separated by a polyurethane spacer of 0.015 inch. The coaxial line was semirigid with a solid outer sheath of stainless steel (0.034 inch in diameter) and a center conductor of copper weld material (0.008 inch in diameter).

A. THERMAL CONSIDERATIONS

A comparison of the thermal conduction for the two cables is given in Figure 23, using two mixer temperatures (4.2 and 77 K). The amount of heat transferred from the external environment (300 K) through the cable to the photomixer (77 K) is seen to decrease asymptotically toward zero as the cable lengths are increased. The advantage of a twin lead can be seen to diminish as greater cable lengths are required. Observing in Figure 23 sheet 1, for 10 cm of cable length, the twin lead transfers 10.2 mW of heat, compared to 28.5 mW for the coaxial cable, while at 20 cm, the twin lead transfers 5 mW and the coaxial cable transfers 14.5 mW. While the ratio of the heat load between the two types of cables remains constant, the difference in the absolute amount of heat transferred was cut in half by increasing the cable length from 10 to 20 cm. Similar results are obtained from Figure 23 sheet 2, for the 4.2 K photomixers.

The heat load of 10 cm of coaxial cable from 77 to 300°K was measured using the thermal mockup of the array structure shown in Figure 24. The measured heat load was 27.8 mW per coaxial cable, agreeing with the calculated value of 28.5 mW.

B. ELECTRICAL CONSIDERATIONS

The variation of electrical loss with cable length is given in Figure 25 for a nitrogen-cooled photomixer and IF frequencies of 150 and 1500 MHz. The coaxial line is seen to have a definite advantage of providing

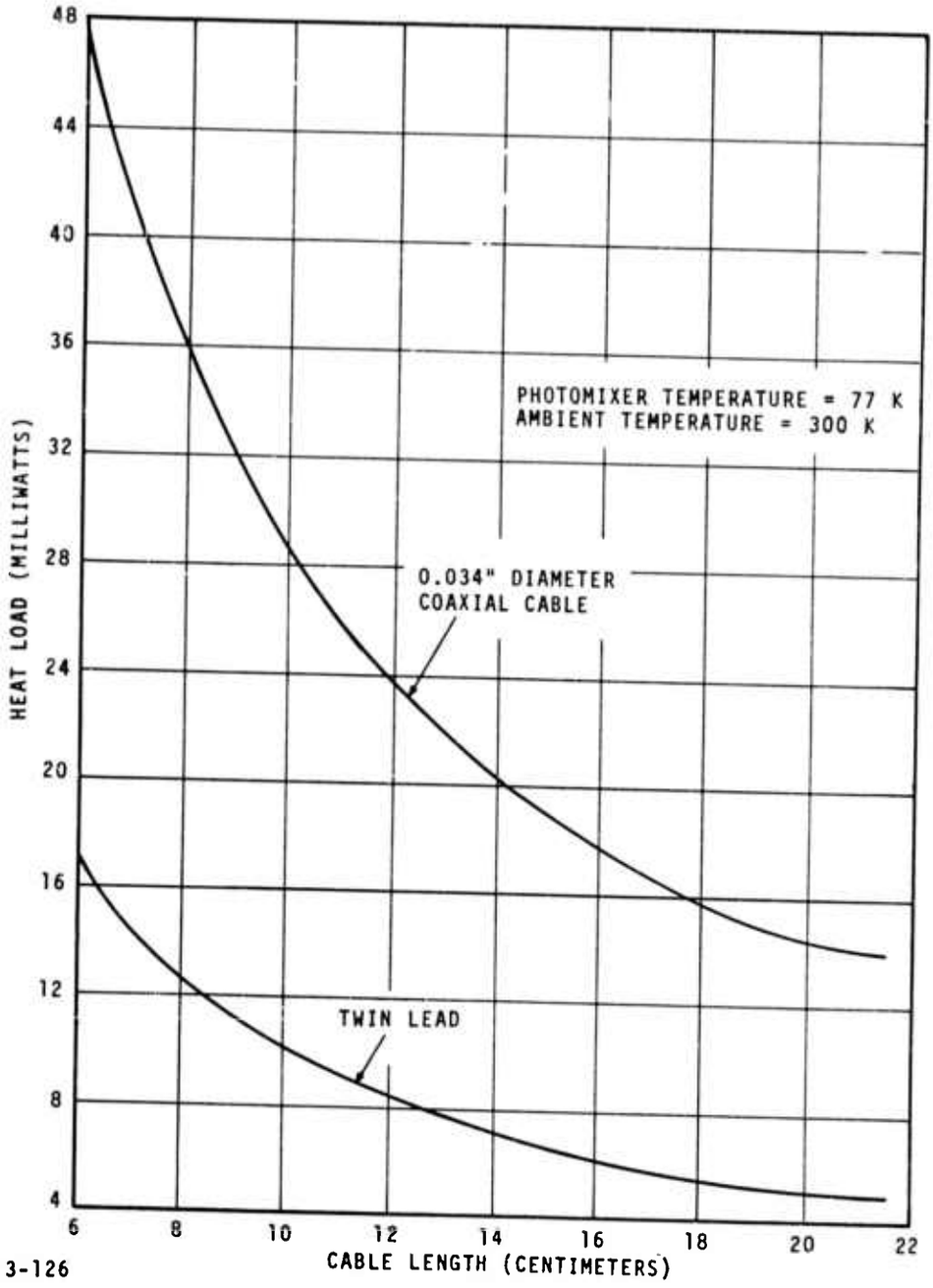

FIGURE 23. CALCULATED HEAT LOAD VERSUS CABLE LENGTH FOR COAXIAL AND TWIN-LEAD CABLES (SHEET 1 OF 2)

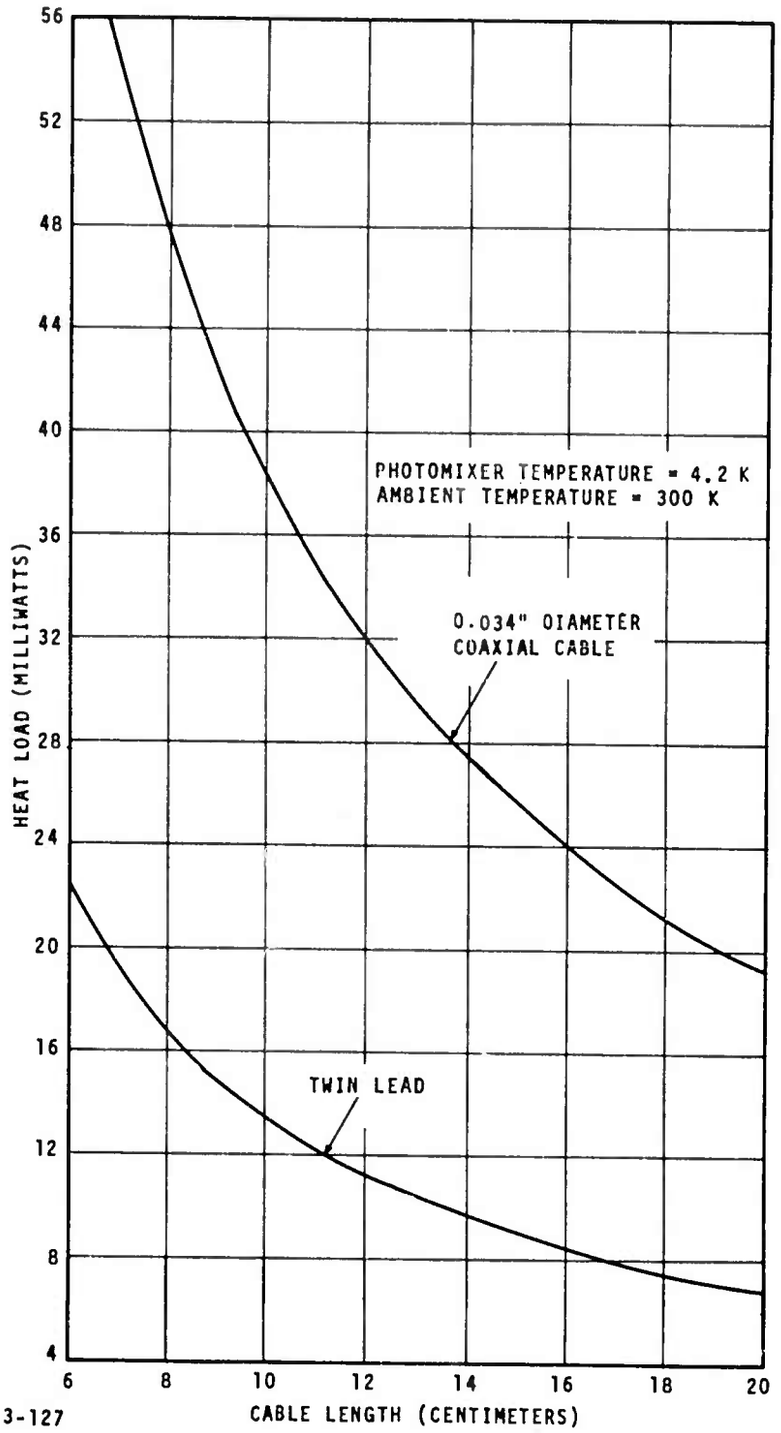

FIGURE 23. CALCULATED HEAT LOAD VERSUS CABLE LENGTH FOR COAXIAL AND TWIN-LEAD CABLES (SHEET 2 OF 2)

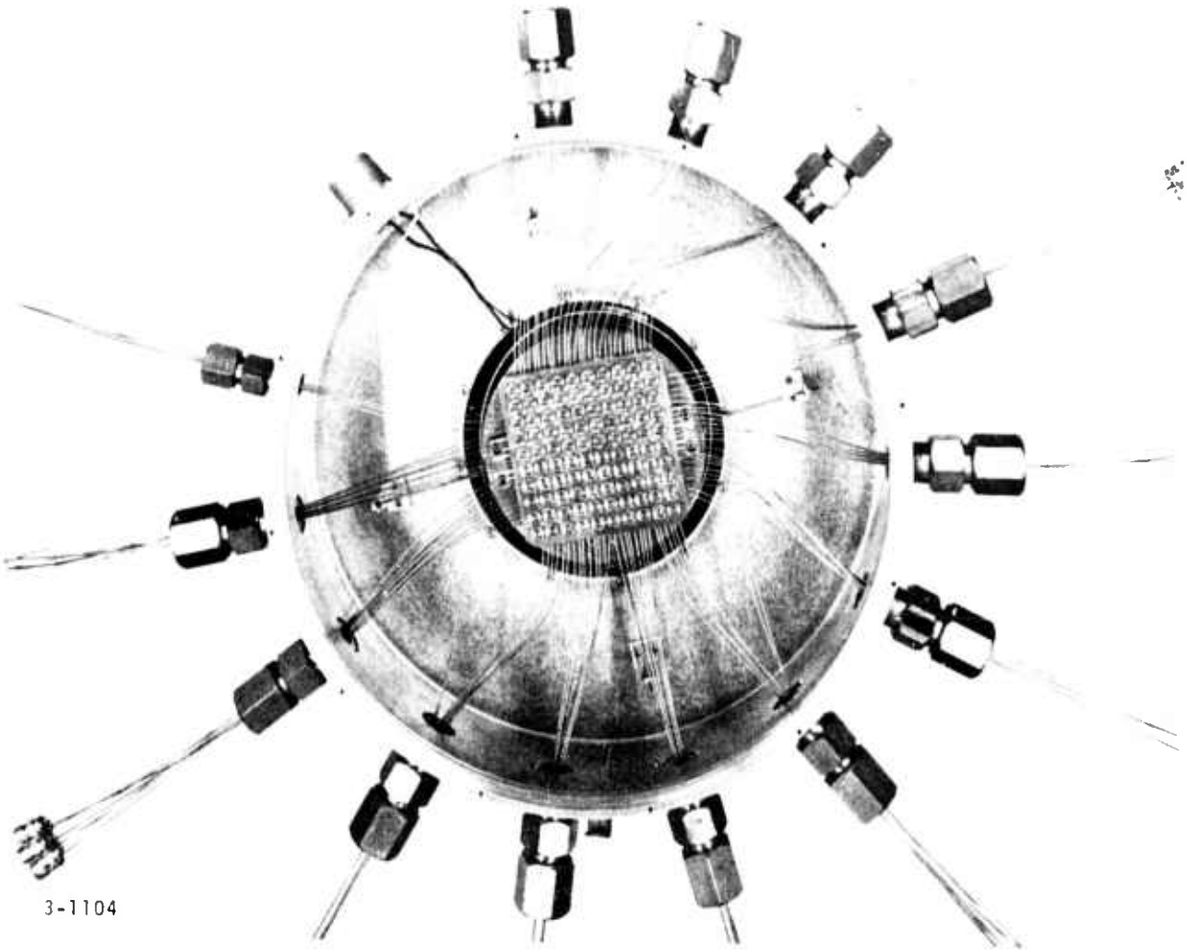

FIGURE 24. 10 × 10 ELEMENT ARRAY STRUCTURE WITH MICROCOAX CABLING

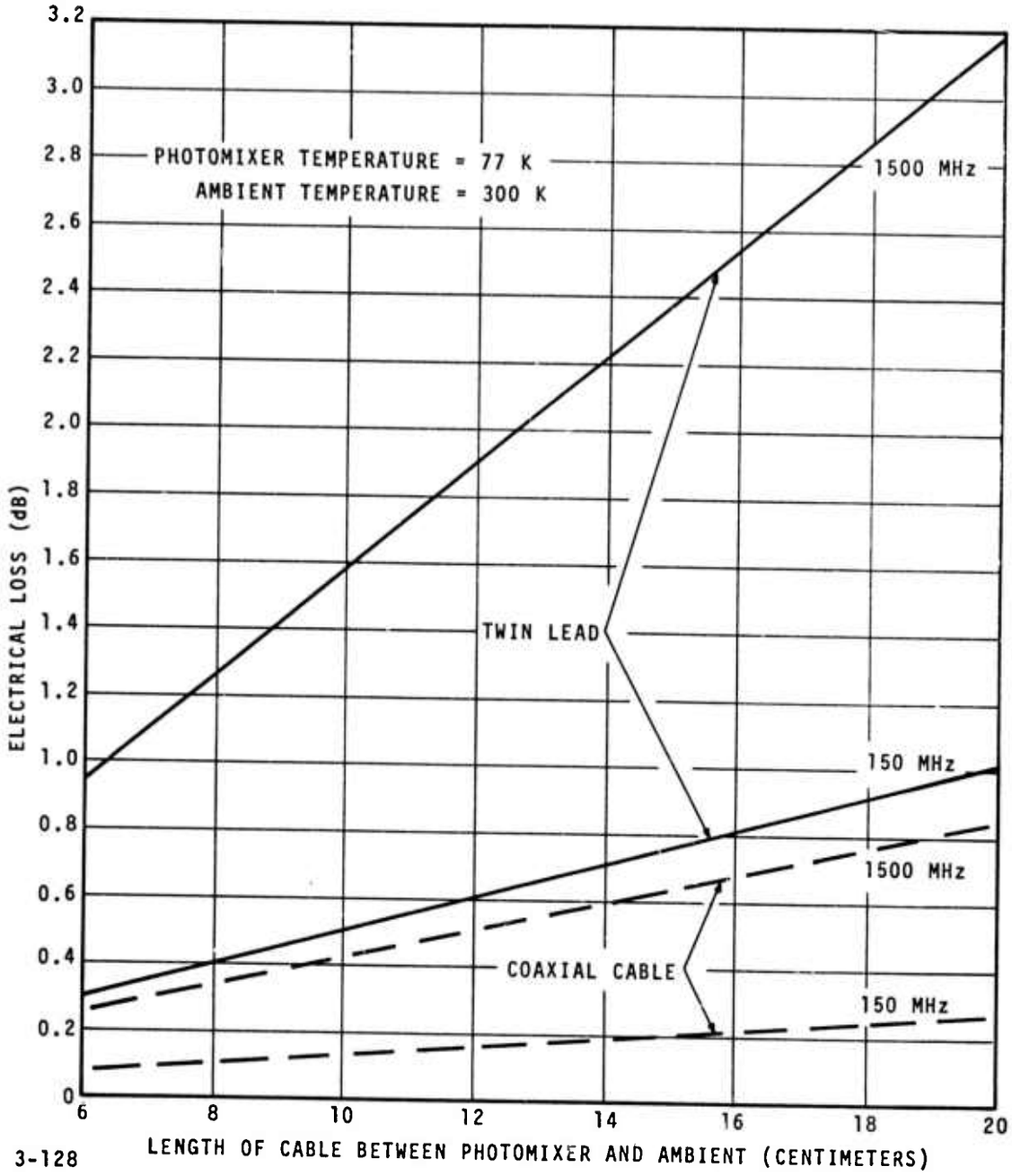

FIGURE 25. CALCULATED ELECTRICAL LOSS VERSUS CABLE LENGTH FOR COAXIAL AND TWIN-LEAD CABLES

lower electrical loss for the particular transmission lines considered between 300 and 77 K. Measurements were carried out on the electrical loss of the 50-ohm coaxial cable and the measurement results are compared to the calculated values in Table 4.

TABLE 4. MEASURED AND CALCULATED ELECTRICAL LOSS OF A 12-FOOT LENGTH OF 50-OHM COAXIAL CABLE*

IF Frequency (MHz)	Electrical Loss			
	Calculated (77 to 300 K)		Measured (300 K)	
	(dB)	(dB/ft)	(dB)	(dB/ft)
150	4.86	0.405	6	0.5
1000	-	-	15	1.25
1500	15.5	1.29	19	1.58

*The stainless steel outer conductor has a diameter of 0.034 inch and a thickness of 0.003 inch. The copper weld inner conductor has a diameter of 0.008 inch.

lower electrical loss for the particular transmission lines considered between 300 and 77 K. Measurements were carried out on the electrical loss of the 50-ohm coaxial cable and the measurement results are compared to the calculated values in Table 4.

At an IF frequency of 1500 MHz, the measured loss was 1.58 dB/ft compared to the calculated value of 1.29 dB/ft. Similarly for an IF of 150 MHz, the measured signal attenuation was 0.5 dB/ft and the calculated value was 0.40 dB/ft. The discrepancy can, in part, be attributed to an approximation made in the calculations whereby it was assumed that the center conductor was composed entirely of copper. In actuality, part of its center core contained a layer of stainless steel. Since the resistivity of copper is lower than steel, the calculated loss will be accordingly lower. In addition, the measured loss was for a 300 K coaxial cable not having the benefit of one end cooled to 77 K which reduced the average loss per unit length.

An analysis of the crosstalk between twin leads was performed for the worst case condition where the two lengths of cross-coupling cables were a quarter wavelength long at the particular IF frequency. The resultant crosstalk for cables separated by twice the conductor spacing was -11.5 dB for the 50-ohm twin lead cable and -13 dB for the 300-ohm twin lead line. The resultant crosstalk measured for the 300-ohm twin-lead cable was -15 dB which was in agreement with the calculated value of -13 dB for cables separated by the same spacing.

For the case of a liquid nitrogen-cooled photomixer and an IF frequency of 1500 MHz, it can be seen that the 50-ohm coaxial line has definite advantages over a twin lead line. A coaxial cable length of 15 cm results in a calculated electrical loss of only 0.63 dB, compared to 2.4 dB for a twin-lead line, and a crosstalk isolation of approximately -100 dB, compared to about -15 dB for a twin-lead line. These advantages more than compensate for the disadvantage of the higher heat load (19 mW) of the coaxial line. Based on these considerations, the coaxial cabling has been chosen for the 77 K, 1500 MHz response heterodyne array.

The crosstalk between mixer channels was then measured using the coaxial cable and the mockup of the array structure. At 1000 MHz the corsstalk was -56 dB and at 1300 MHz the crosstalk was -42 dB. These values of crosstalk are very low and will introduce no difficulty when the array is implemented.

V. INITIAL DESIGN OF A 10 × 10 1.5 GHz PV-HgCdTe ARRAY

A. OPTICAL REQUIREMENTS

1. TELESCOPE

Located in the focal plane of the receiving telescope is a microlens array composed of a 10 × 10 element matrix array of square lenses with the dimensions of a single imaging element being 0.8 × 0.8 cm. To obtain the highest resolution for the imaging system the array must be used in conjunction with an f/300 diffraction-limited telescope whose diffraction-limited airy disc in the focal plane is just matched to a single microlens. The field of view (FOV) of such an optical system is:

$$\theta_{FOV} = 2.44 \frac{\lambda}{D} \tag{5}$$

where

θ_{FOV} = field of view of a single element of a heterodyne array and is defined between the -4.3 dB crossover points of the imaging array pattern as shown in Figure 21

λ = 10.6 μm

D = telescope collecting aperture diameter

This relationship is shown plotted in Figure 26. As shown, the telescope collecting aperture of 0.26 m is required for 100-μrad single-element FOV or 2.6 m for a 10-μrad single-element FOV. From this it can be seen that the size and weight of the imaging system are very heavily dependent upon the resulution requirements that are imposed upon the system since both the large aperture diameter and high f/number must be provided for.

We can estimate the relative distance from the output of the optical telescope to the 10 × 10 element array, assuming a collimating type telescope with the reduced beam size at the output of the telescope matched to the dimensions of a single microlens. The minimum distance between the telescope and the array is the Rayleigh range of the effective telescope

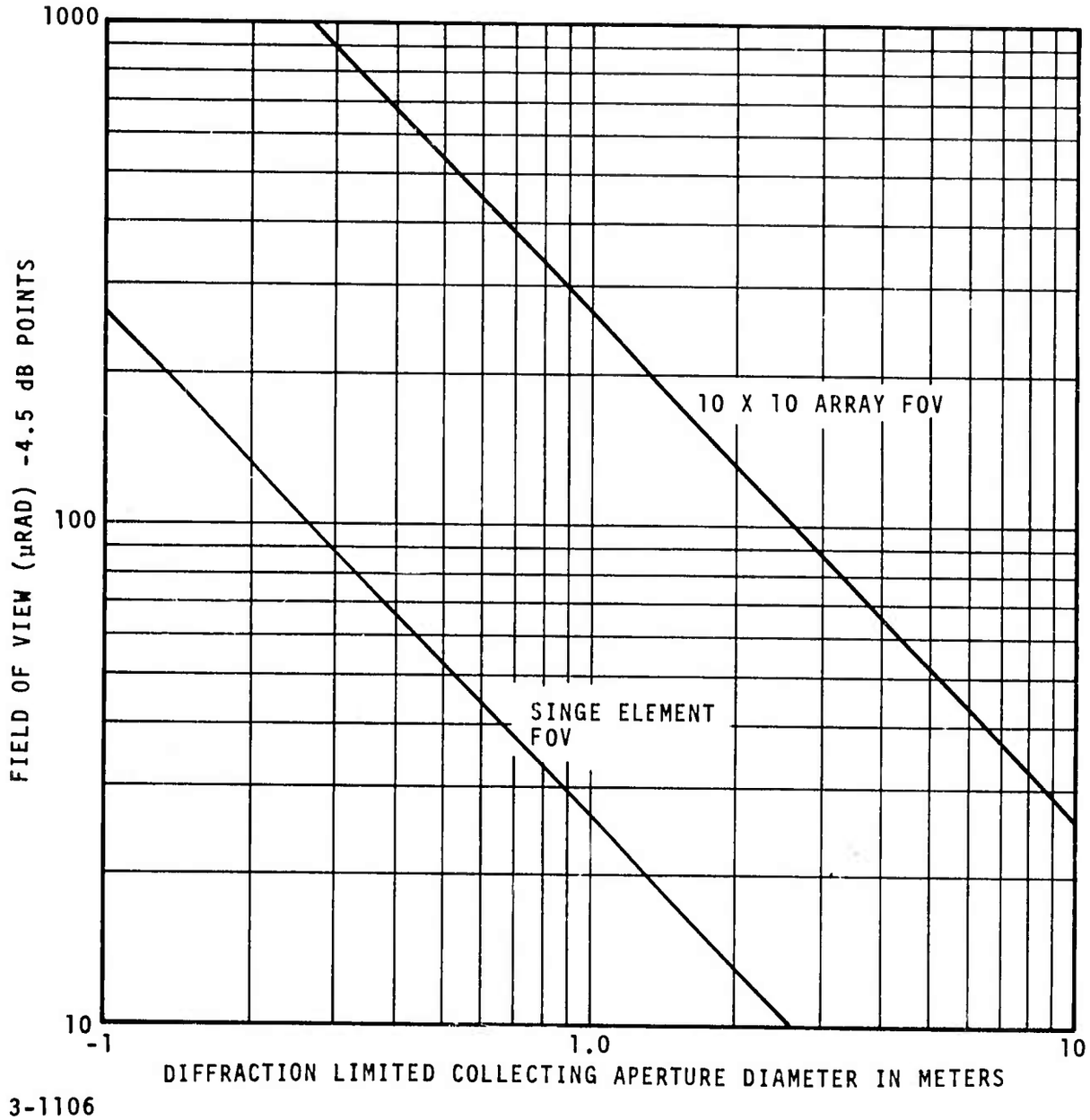

FIGURE 26. SINGLE-ELEMENT FOV FOR f/300 TELESCOPE

output aperture. This is obtained from reference 6 which states that at the distance $D^2/2\lambda$ the phase error introduced leads to negligible deterioration of the image and that a diffraction pattern at $D^2/2\lambda$ is as good as that at an infinite distance. Then for a 0.8 cm effective output aperture the Rayleigh distance is 3 m. This distance is quite long for a 100-μrad beam system, but can be made more compact by the use of a beam folding technique. However, when compared to the size of a telescope used for the 10-μrad beam system it is relatively short and will not significantly affect the size of the overall system.

2. LASER LO

The laser LO power was determined to be 2 mW/mixer element in Appendix B for 77 K, 1500-MHz operation of PV-HgCdTe photomixers. Therefore, 200 mW of plane wave uniform phase front 10.6-μm laser radiation is required to uniformly illuminate the 8 × 8 cm acceptance area of the microlens array. This size beam will require a collimating telescope to expand the laser LO beam as well as an aspheric lens system to convert the gaussian amplitude shaped laser output to a uniform intensity distribution without affecting the uniform phase front.

B. ARRAY AND COOLER PACKAGE

The array package is shown in Figure 27. It is composed of a liquid nitrogen dewar in which is mounted the mixer 10 × 10 element mixer array structure. The structure is shown in Figure 25 with the bottom plate of the dewar removed. On the array structure are mounted 100 detector mounting bases similar to the one seen in Figure 28. 100 coaxial cables (0.034 in. OD) can be seen connecting the perimeter of the dewar to the array structure. These cables are individually routed through the array structure to a particular feedthrough from one of the detector mounting bases. The routing as shown in Figure 29 shows the underside of the array structure. The individual coaxes and the attachment to the detector mounting bases are fully shielded from each other, resulting in the very low electrical cross-talk measured between the mixer channels.

Thermal tests were conducted with the fully assembled array package and the simulated laser LO heat load. Under full load the dewar (3 liters of liquid nitrogen capacity), provided an operating time of 25.5 hours. If an operating time longer than this is required, a closed-cycle cooler capable of operating in the 80 K region is available providing up to 5 W of cooling in a package the same size and weight as the dewar tested. This cooling should be adequate to handle the 0.2 W of laser LO and the 2.8 W of heat leak due to the coaxial cables.

3-1105

FIGURE 27. 10 × 10 WIDEBAND (10 TO 1500 MHz) HETERODYNE IMAGING ARRAY PACKAGE

FIGURE 28. PV-HgCdTe DETECTOR MOUNTING BASE

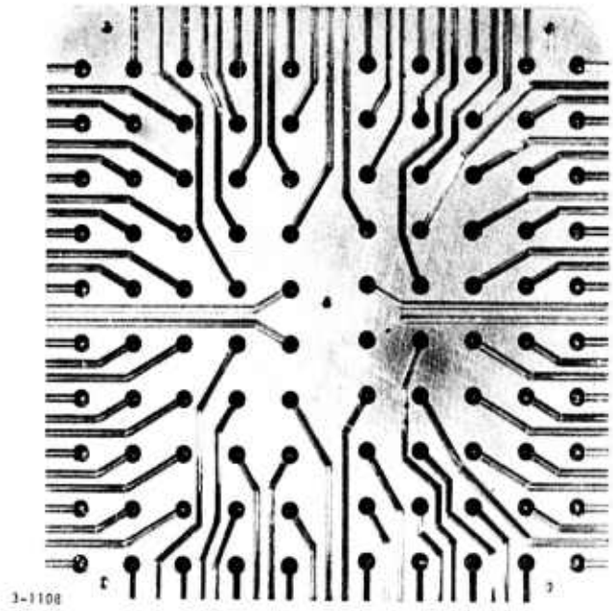

FIGURE 29. UNDERSIDE OF 10 × 10 ARRAY STRUCTURE

VI. 4.2-K COOLER REQUIREMENTS FOR A 100-ELEMENT GERMANIUM ARRAY

A. LO AND DC BIAS POWER REQUIREMENTS FOR NEAR-QUANTUM NOISE-LIMITED OPERATION

A matrix array design for Ge:Cu (Sb) heterodyne mixer elements has been developed under a previous program, N00014-68-C-0273, entitled "Advanced Capability Infrared Receiver System." This program developed a high frequency array structure capable of employing heterodyne mixer elements in a 10×10 configuration. This design was implemented on a smaller scale in a subsequent program, N00014-70-C-0407, where a 2×2 array was built incorporating a microwave integrated circuit impedance matching network to provide the optimum high frequency performance. Based upon the array performance measured during this program, we can predict with reasonable certainty the receiver sensitivity as a function of the dc bias and local oscillator power dissipated in the mixer element.

Figure 30 shows the predicted system NEP's at 150 and 1500 MHz for a single channel of an array including the optics losses, mixer quantum efficiency, impedance matching network, and second stage noise contributions due to the preamplifier and associated signal processing electronics. The individual mixer impedances are approximately 1000 ohms with the application of 50 mW of 10.6 μm LO power. From this we can see that a total of 200 mW (150 mW dc bias plus 50 mW LO) is required per array element in order to obtain a sensitivity of 2.2×10^{-19} W/Hz at an IF frequency of 1500 MHz. Significant decreases in the dissipated power can be obtained to more reasonably meet the present capabilities of coolers at 4.2 K providing that the system sensitivity can be degraded slightly. As an example, the thermal requirements can be reduced to 100 mW per array element if the total system is capable of operating with its overall system sensitivity of 4.7×10^{-19} W/Hz at the highest IF frequency (1500 MHz).

If the bandwidth requirement of the system is only 150 MHz, which would adequately provide for a signal from a moving aircraft, the overall system sensitivities can be improved to 1.55 and 2.7×10^{-19} W/Hz, for total (LO and dc) bias powers of 200 and 100 mW, respectively.

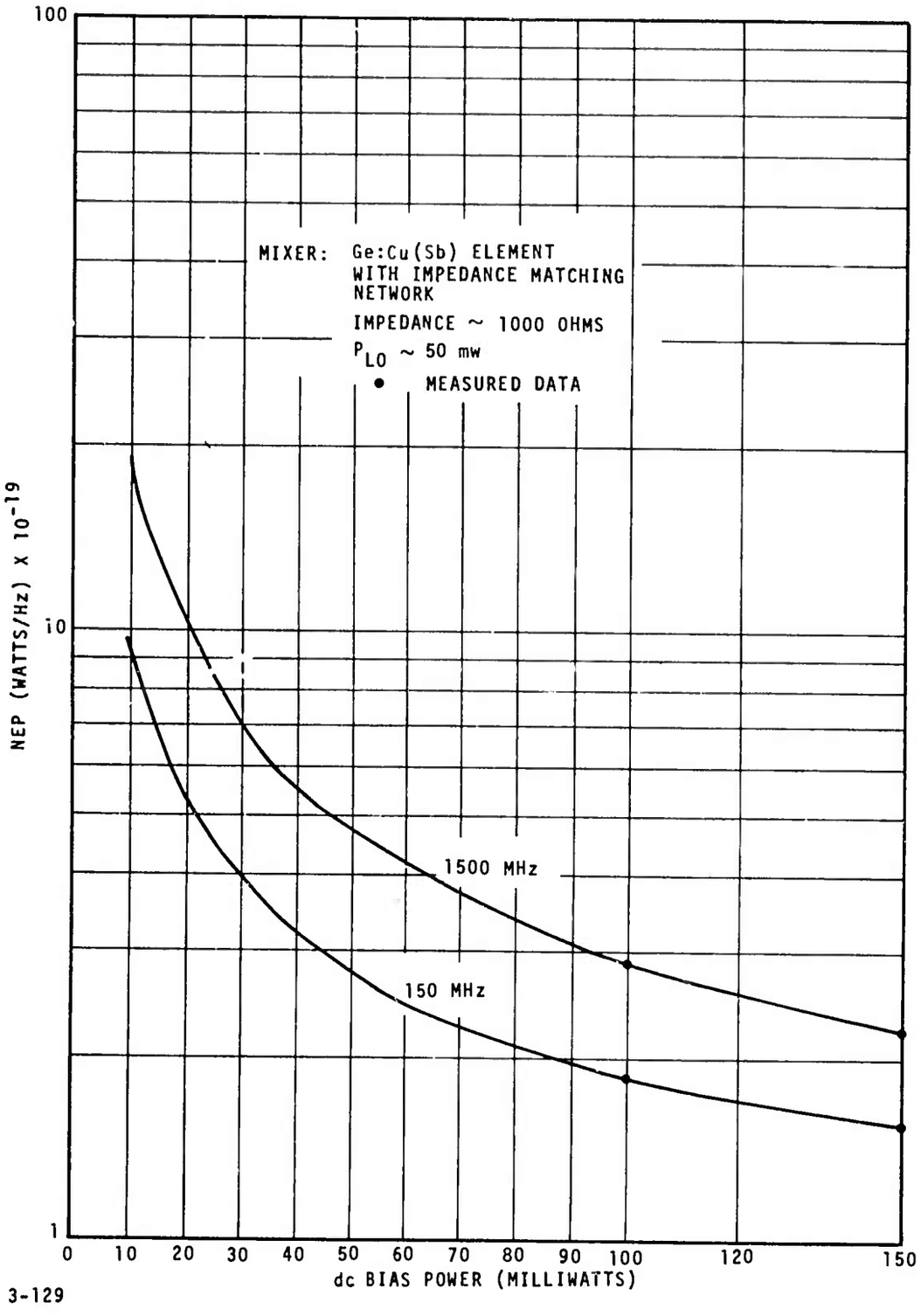

FIGURE 30. PREDICTED NEP VERSUS DC BIAS POWER FOR A TYPICAL WIDEBAND Ge:Cu (Sb) RECEIVER AT 10.6 μm

A system which was designed to operate over a 150-MHz bandwidth could be expected to produce system NEP's which are a factor of two more than the wideband system data for 150 MHz shown in Figure 30 and would require less LO power.

Using the appropriate approximations, overall system sensitivities of 1.1×10^{-19} and 2.2×10^{-19} W/Hz are predicted for total power dissipations of 100 and 50 mW, respectively. These results are summarized in Table 5 which gives the expected sensitivity per channel of a 10×10 array with the LO and dc bias thermal load.

B. DETERMINATION OF THE TEMPERATURE RISE AT THE CENTER OF 10×10 GERMANIUM PHOTOMIXER ARRAY

As in the preceding analysis, the temperature differential at a point can be determined by the sum of the thermal resistance between the point in question and the heat sink multiplied by the heat load applied. In the case of the 10×10 element mixer array surrounded by a 4.2 K heat sink, we assume a temperature maximum to occur at the center of the array. In setting up our model of the heat flow for this array, the following assumption is made: because of the imperfect interfaces between the rows of the array, the primary heat flow will occur along the horizontal direction for each individual layer of detectors. A single row of the detector array is represented by the thermal resistances in Figure 31. The

TABLE 5. PREDICTED SYSTEM PERFORMANCE USING A COPPER-DOPED GERMANIUM PHOTOMIXER

System Bandwidth (MHz)	System Sensitivity Per Channel (W/Hz)	4.2 K Array Cooler Requirements (W)
1500	2.2×10^{-19}	20
1500	4.7×10^{-19}	10
150	1.1×10^{-19}	10
150	2.2×10^{-19}	5

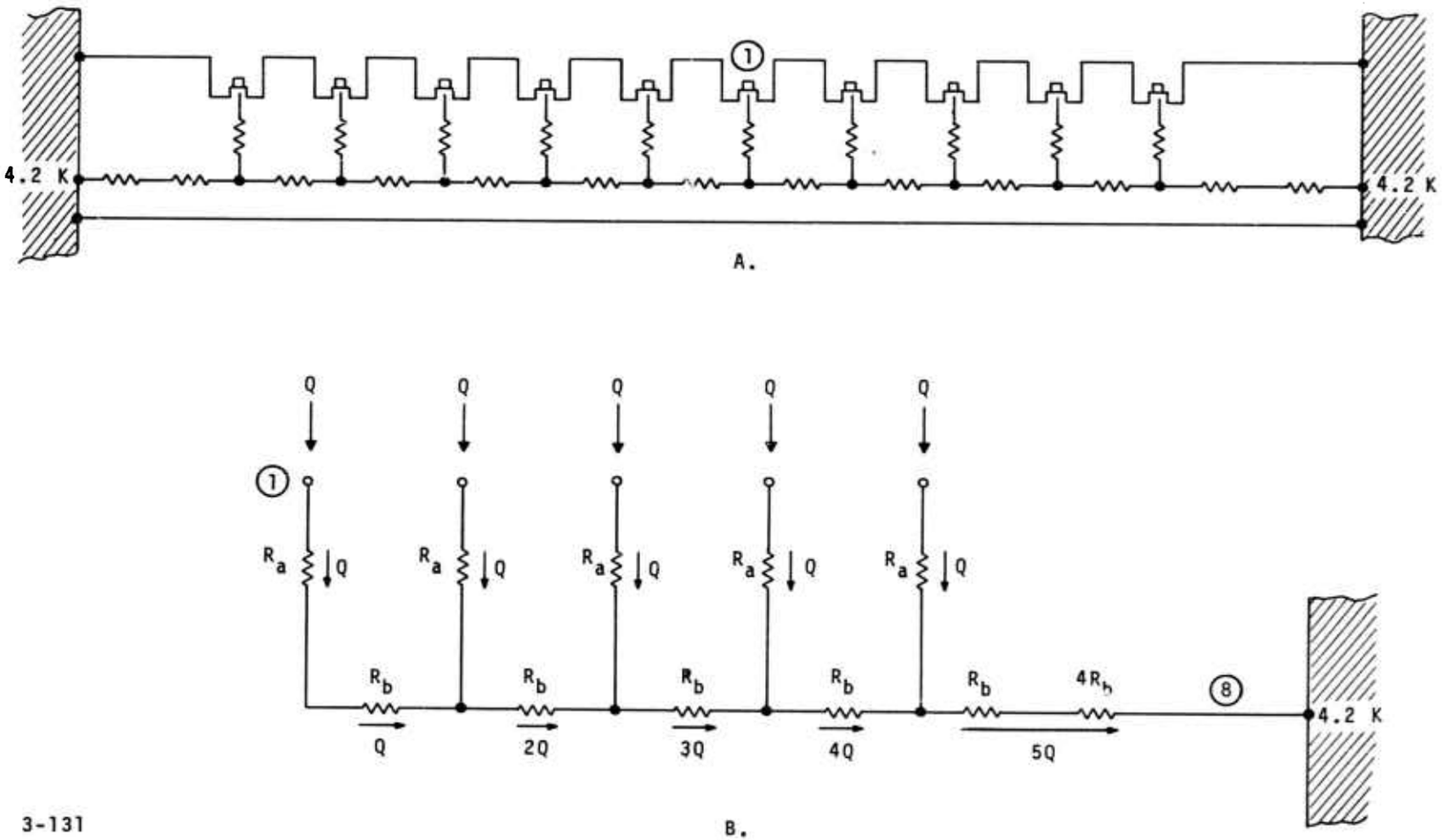

FIGURE 31. DETECTOR MODULE FOR A 4.2-K Ge DOPED PHOTOMIXER ARRAY OF 100 ELEMENTS (10 × 10 CONFIGURATION)

heat input to each detector is represented by Q. Because of symmetry with respect to the center of the row, only half the row need be considered. The temperature developed at the most interior detector is calculated from thermal resistances $R_a = 0.37$ K/W and $R_b = 1.3$ K/W with thermal loads (LO and dc bias) of 150 mW per detector. The sum of the temperature differentials from point 1 to point 8 (heat sink at 4.2 K) results in a temperature rise of 6.8 K at this interior detector. The absolute temperature at this point then reaches 11 K in the steady state case.

The temperature rise to 11 K of an antimony-compensated germanium photomixer is expected to degrade the frequency response but not sensitivity level below the cutoff frequency of the mixer element. We can estimate this degradation in frequency response and sensitivity degradation from reference 7 which shows a plot of response time (τ) as a function of applied electric field for a compensated germanium photomixer at 5 and 21 K. The response time degradation over the 16 K temperature interval is approximately $1.35\ \tau_{5\ K}$. Approximating the temperature dependence, we calculate a behavior of $\tau \sim T^{0.2}$ so that the response time degradation will be on the order of $1.17\ \tau_{5\ K}$ with a corresponding 15-percent lowering of the cutoff frequency.

Reference 7 also contains a plot of carrier mobility as a function of temperature for a partially compensated germanium detector. From 5 to 11 K, the degradation of mobility was observed to be approximately 15 percent. From equations 6 and 7 for mixer conversion gain (G) and NEP, we get:

$$G = \frac{\eta q \mu \tau}{2h\gamma_2 (1 + \omega^2 \tau^2)} \left(\frac{V}{L}^2 \right) \tag{6}$$

$$NEP = \underbrace{\frac{2\ h\nu_s B}{\eta}}_{\substack{\text{quantum noise} \\ \text{term}}} + \underbrace{\frac{K (T_m + T'_{IF})\ B}{G}}_{\substack{\text{degradation from quantum} \\ \text{noise-limit term}}} \tag{7}$$

where

μ = carrier mobility

τ = mixer time constant

We can see that τ enters the gain expression in two places. The first is the frequency response which affects the gain as $1/(1 + \omega^2 \tau^2)$. The second is the $(\mu\tau)$ product which affects the conversion gain at all frequencies. From this we can conclude that to a first approximation, the gain is unaffected below the cutoff frequency since the mobility decreases by $\sim$15 percent and the time constant increases by $\sim$15 percent leaving the $\mu\tau$ product approximately unchanged.

VII. CONCLUSIONS

1. An initial design for a 10 × 10 element matrix array has been developed assuming 1500-MHz operation and the use of 77 K photodiodes.

2. Thermal analyses of the PV-HgCdTe and the Ge:Cu (Sb) array structures determined that the thermal loading due to LO and dc bias power will have a minimal affect on the photomixer sensitivities.

3. Array NEP's of better than 1.9×10^{-19} W/Hz can be obtained out to 300 MHz for five loosely specified PV-HgCdTe photomixers.

4. Matched mixer channel responsivities have been obtained using the mixer bias level and amplifier gain balancing parameters.

5. There is greater than 30-dB isolation between adjacent mixer channels up to 1500 MHz in the PV-HgCdTe 10 × 10 matrix array structures.

6. Image plane dissection techniques were investigated with batch processing of germanium lenses and molding of GeSbSe infrared glass proving the most feasible.

7. LO powers of 0.5 to 2.0 mW are required for near-quantum noise-limited operation of PV-HgCdTe photomixers from 10 to 150 MHz and from 10 to 1500 MHz.

8. 0.034-inch OD semirigid cable is a good choice for the high density cabling needed for a 10 × 10 matrix array operating from 10 to 1500 MHz.

APPENDIX A

LASER LO POWER REQUIREMENTS FOR PV-HgCdTe

It has been shown (reference 8) that for a PV-HgCdTe photomixer operating in the flat portion of its frequency response ($f/f_c \ll 1$), quantum noise-limited heterodyne operation is obtained when:

$$I_o >> \frac{2k\,(T_m + T'_{IF})\,G_D}{q} \tag{1}$$

or

$$P_{LO} >> \frac{2k\,(T_m + T'_{IF})\,G_D\,h\nu}{q^2\,\eta} \tag{2}$$

where

I_o = dc photocurrent induced by the laser LO

k = Boltzmann's constant

T_m = physical temperature of the photomixer

T'_{IF} = effective input noise temperature of the IF preamplifier

G_D = small-signal shunt conductance of the photomixer

q = electronic charge

h = Planck's constant

ν = infrared frequency

η = photomixer quantum efficiency

When the terms on the left and right side of equations 1 or 2 are equal, the thermal noise of infrared mixer and IF amplifier degrades the receiver sensitivity by 3 dB.

Calculated and measured data on 10.6-μm heterodyne receivers at AIL (reference 8) indicate that a properly designed heterodyne receiver can exhibit quantum noise-limited operation for approximately 1 to 2 mW of incident laser LO power illuminating the PV-HgCdTe photomixer. Since photo-induced shot-noise must overcome the thermal noise of the photomizer and IF preamplifier, it is important to select a preamplifier which allows maximum transfer of shot noise so that the ratio of shot to thermal noise is maximized.

The measured receiver NEP as a function of incident LO power at an IF of 30 MHz is shown in Figure 32 for a PV-HgCdTe photomixer. In order to achieve quantum noise-limited operation, it was necessary to operate with approximately 1.5 mW of LO power incident upon the mixer. Photo-induced shot-noise exceeded the thermal noise for these values of LO power ensuring quantum noise-limited operation and optimum receiver sensitivity.

By using the PV mixer design equation from reference 8, we can obtain curves of the receiver NEP versus LO power for typical values of mixer parameters and IF frequency. The equation for NEP is:

$$NEP = \frac{hvB}{\eta} \left\{ 1 + \frac{2k\,(T_m + T'_{IF})\,h\nu}{q^2\,\eta\,P_{LO}} \left[G_D\,(1 + R_s\,G_D) + \omega^2\,R_s\,C_D^{\,2} \right] \right\} \tag{3}$$

where

$T_{IF} = \left(F_{IF} - 1 \right) T_o$

P_{LO} = LO power

B = IF bandwidth

R_s = series resistance of diode

C_D = junction shunt capacitance

ω = IF

NF = noise figure of IF amplifier

G'_{out} = source conductance

F_{IF} = IF amplifier noise factor

T_o = reference temperature

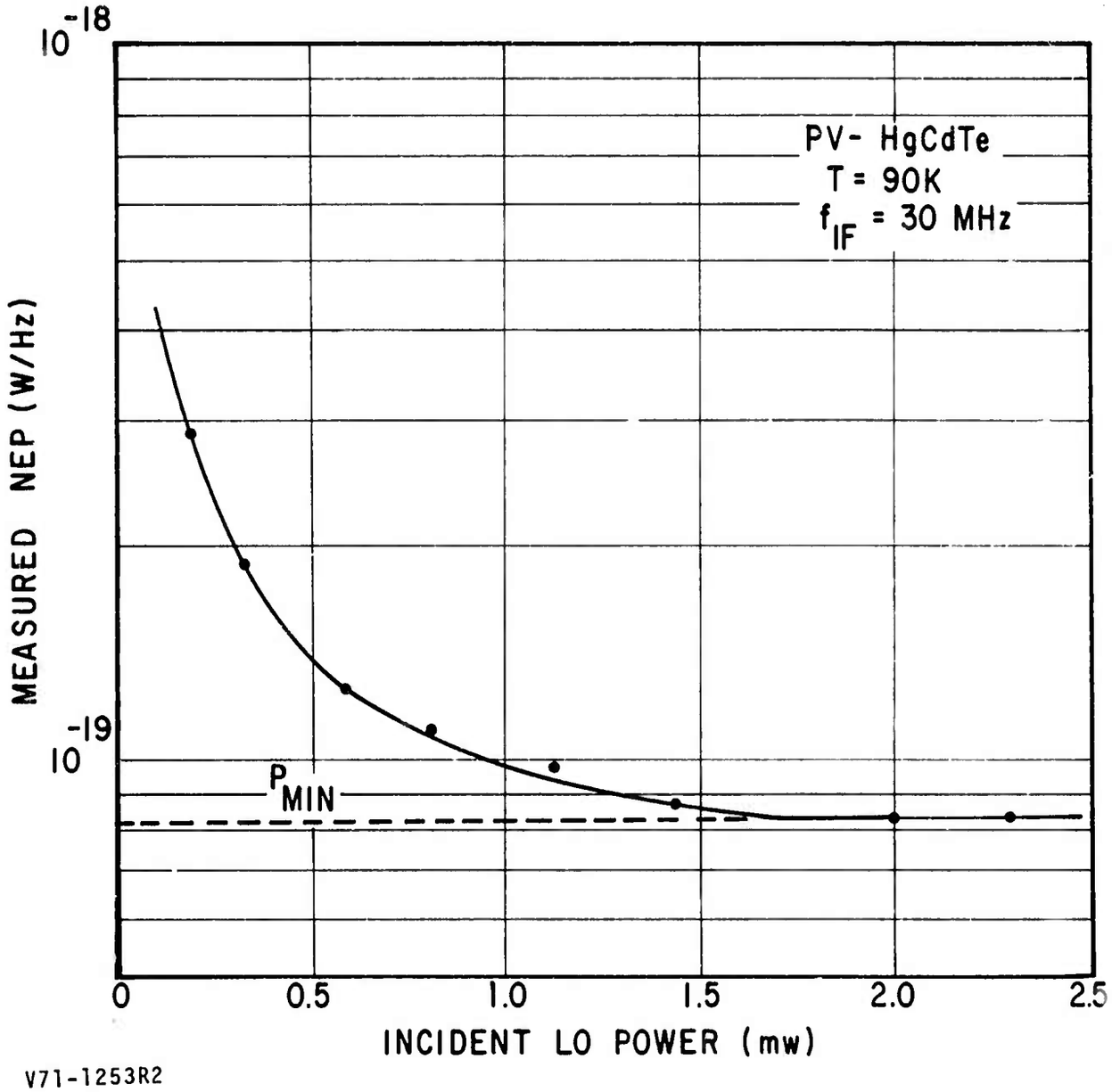

FIGURE 32. MEASURED RECEIVER NEP AS A FUNCTION OF LOCAL OSCILLATOR POWER

The terms of interest for obtaining the LO power requirements are η, NF, G_D, R_s, and C_D. F_{IF} is the noise of the IF preamplifier which must be minimized to obtain a low effective input noise temperature of the IF amplifier. This, however, is limited by the state of the art of wideband IF preamplifiers and has a value which varies with the instantaneous IF bandwidth requirements of a particular system. We can assign typical values for the noise figure of 5.0 dB for a 1500-MHz and 2.5 dB for a 150-MHz bandwidth IF preamplifier. The remaining parameters are constants for a particular PV-HgCdTe photomixer. From reference 9 we can obtain the typical values of these parameters for high cutoff frequency PV-HgCdTe mixers as follows:

$$\eta = 25 \text{ percent}$$

$$G_D = 10^{-3} \text{ mho}$$

$$R_s = 10 \text{ ohms}$$

$$C_D = 8 \text{ pF}$$

Using these values and the 1500-MHz amplifier noise figure of 5 dB we can predict the NEP of the wideband mixer-preamplifier combination as a function of LO power and IF frequency. There are, however, several partially compensating errors which were assumed in this analysis. The first is that the mixer capacitance is assumed to be a constant. This is an error since, as the detector is reverse-biased, the capacitance decreases thereby yielding a higher cutoff frequency detector with better NEP at the higher frequencies. The second assumption is the case of high quantum efficiency detectors which assumes that the detector is capable of producing as much photo-induced current, I_o, as is predicted by the LO power and equation 4,

$$I_o = \frac{\eta q}{hv} P_{LO} \qquad (4)$$

There is a saturation effect which occurs at high photo-induced current corresponding to a decrease of quantum efficiency and accordingly degraded NEP.

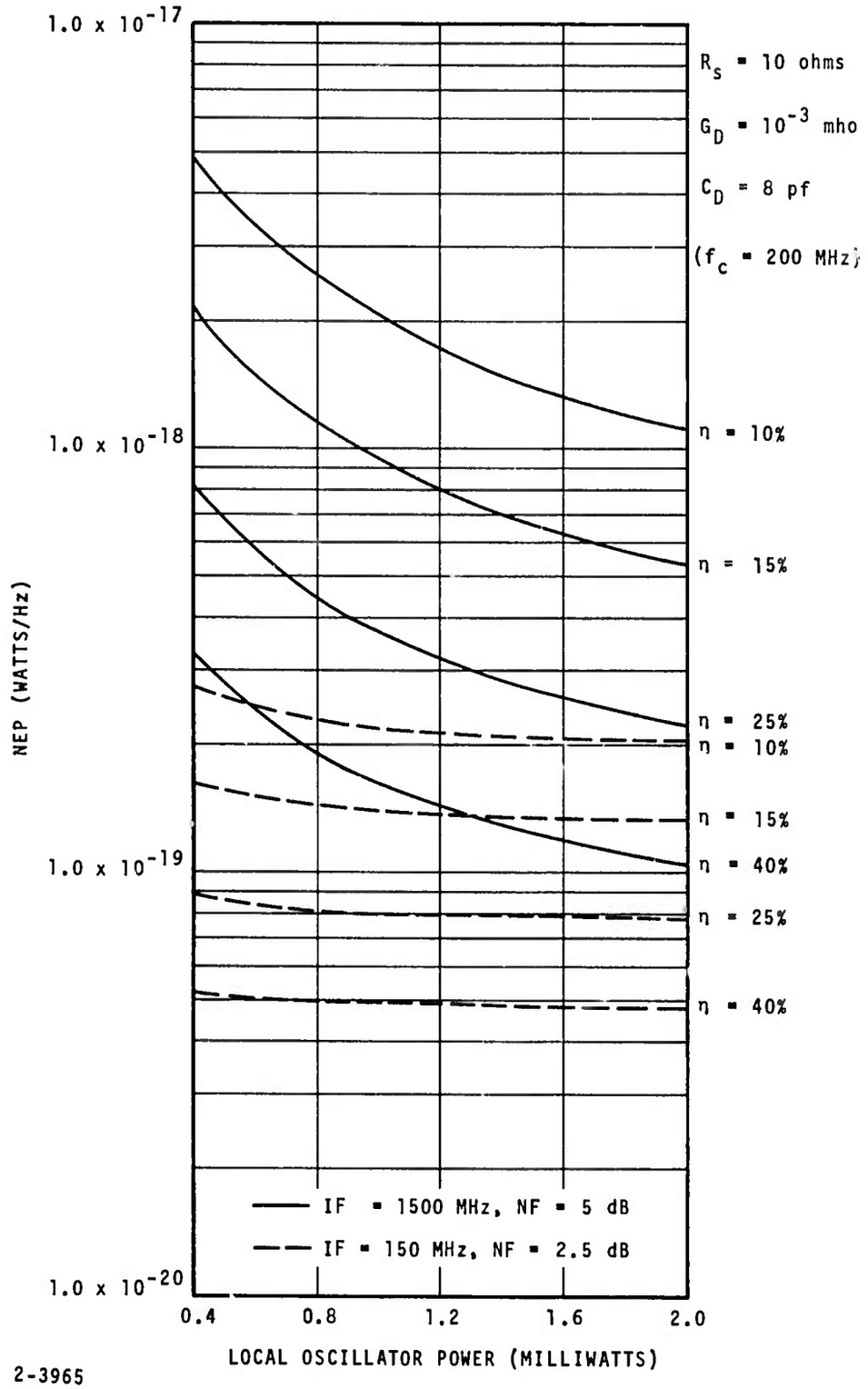

FIGURE 33. NEP VARIATION WITH LO POWER VERSUS QUANTUM EFFICIENCY

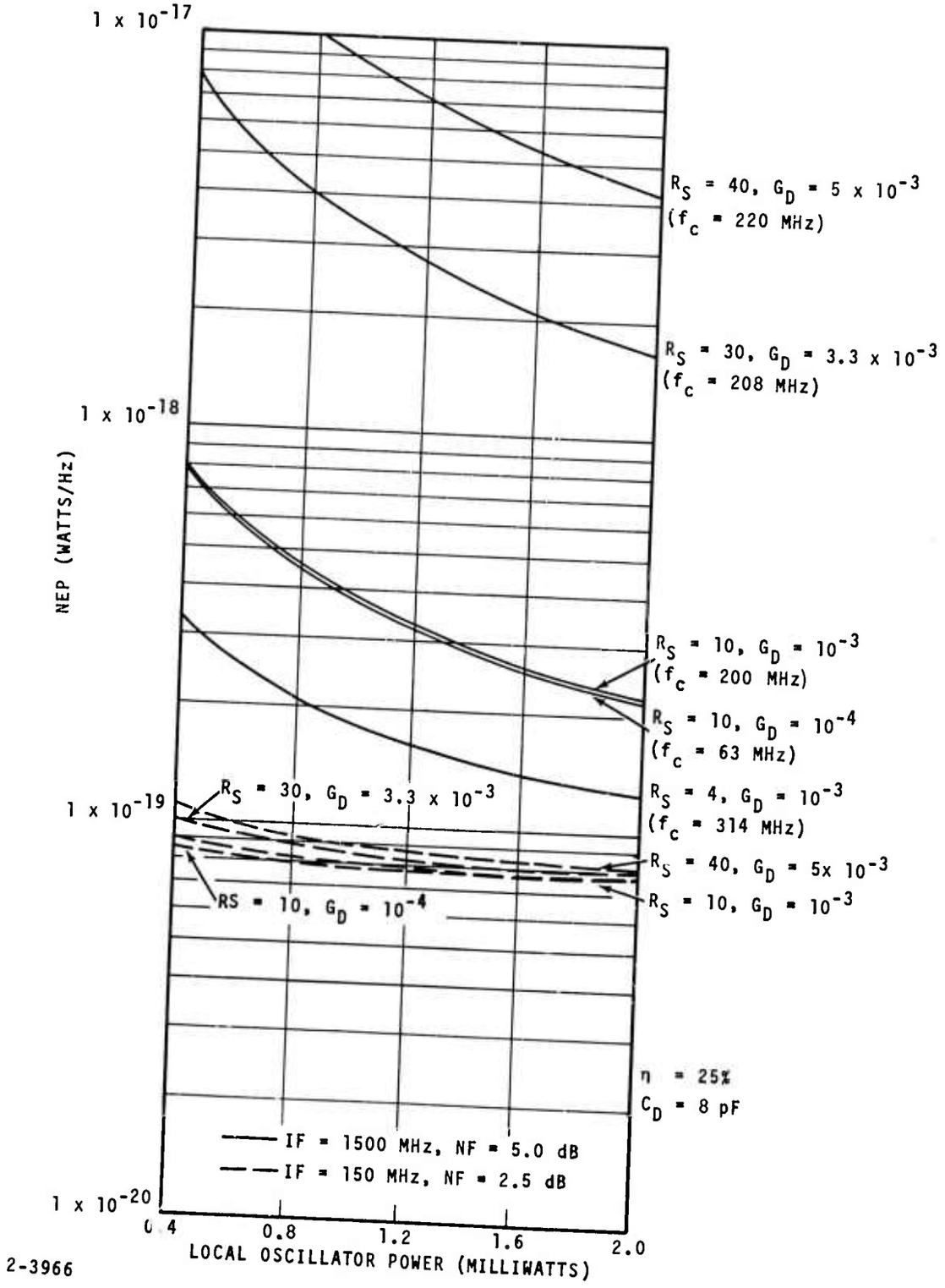

FIGURE 34. NEP VARIATION WITH LO POWER VERSUS (R_S . G_D)

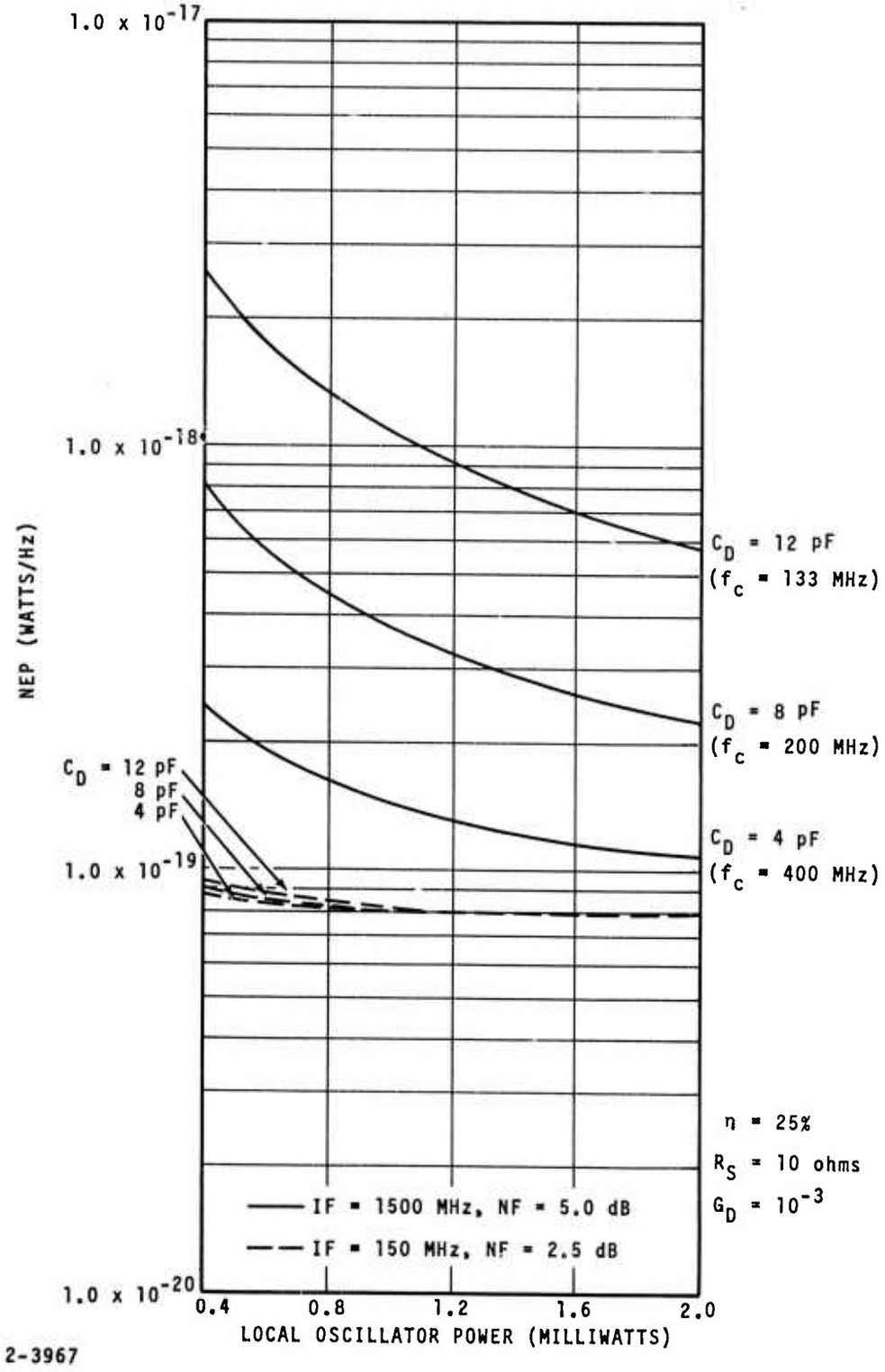

FIGURE 35. NEP VARIATION WITH LO POWER VERSUS MIXER CAPACITANCE C_D FOR $R_s G_D = 10^{-2}$

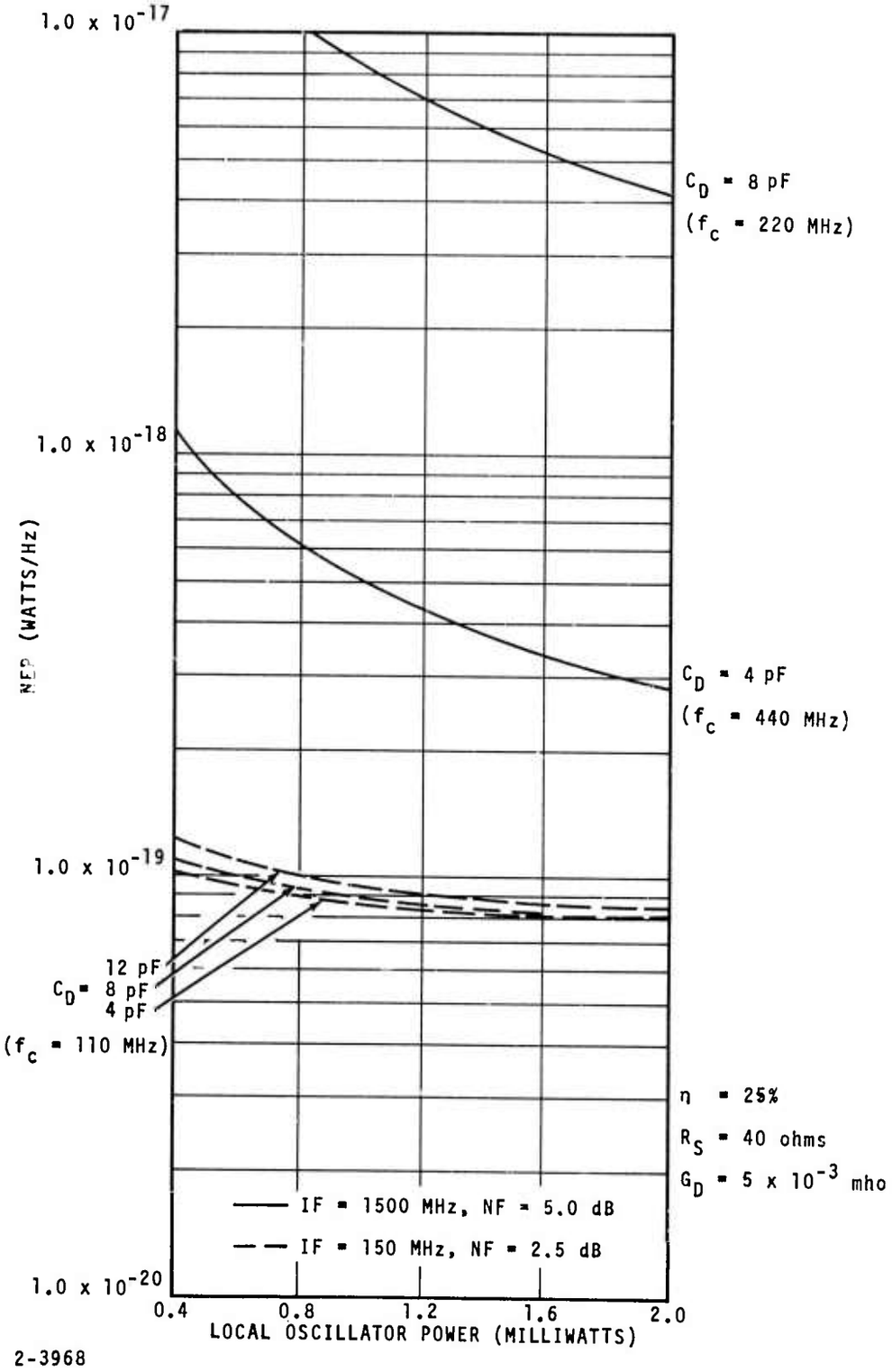

FIGURE 36. NEP VARIATION WITH LO POWER VERSUS MIXER CAPACITANCE C_D FOR $R_S G_D = 0.2$

The analysis is not capable of dealing with these two factors in that they vary greatly from detector to detector. However, since they are partially self-compensating, we use these assumptions to obtain a close approximation to the actual variation of system NEP with LO power for a reasonable range of mixer parameters.

Figures 33 through 36 are a set of parametric curves obtained from equation 4 showing the NEP variation with local oscillator power for various combinations of R_s, G_D, η, and C_D evaluated at 150 and 1500 MHz. A careful examination of these curves will indicate that:

- For mixers operating at 150-MHz bandwidth, the primary consideration for achieving near 10^{-19} W/Hz sensitivity is quantum efficiency. For mixers with quantum efficiencies greater than 15 percent, LO power of 0.5 milliwatts or less will be sufficient
- If sensitivity to 1500 MHz is required, the R_s G_D product must be less than 10^{-2}, the quantum efficiency greater than 25 percent, the diode capacitance less than 8 pF, and the LO power requirement from 1 to 2 mW
- A high quality diode with good front to back ratio (R_s G_D <<1) will have good sensitivity well beyond its cutoff frequency providing $G_D < 10^{-3}$ because the mixer available conversion gain G is inversely proportional to G_D

$$G \approx \frac{C}{G_D} \cdot \frac{1}{1+\left(\frac{f}{f_c}\right)^2} \qquad (5)$$

APPENDIX B

ARRAY PATTERN SYNTHESIS

Referring to Figure 12 of paragraph A, Section III, consider the received signal that is focused by the telescope and the matching lens. For convenience, we shall consider this lens combination as a single unit with the focal length and therefore the f/number of the telescope magnified by the ratio of the two focal lengths, such that,

$$f_1 = f_{\text{telescope}} \left(\frac{f_{\text{telescope}}}{f_{\text{matching lens}}} \right)$$

Then from reference 10, the electrical field distribution of the signal in the plane of the image-dissection lens array is given as:

$$I_o = A 2\pi a^2 \frac{J_1 \left\{ \frac{ka}{f_1} \left[(x + x')^2 + (y + y')^2 \right]^{1/2} \right\}}{\frac{ka}{f_1} \left[(x + x')^2 + (y + y')^2 \right]^{1/2}} \qquad (1)$$

The terms of the expression are defined in Figure 37 which shows the coordinate system used for the array pattern synthesis. This expression describes a diffraction field of the form $J_1(x)/x$ in two dimensions with the center of the pattern displaced from the optical axis by a distance (x', y'). This represents the position of the center of a target that has moved from the optical axis of the telescope.

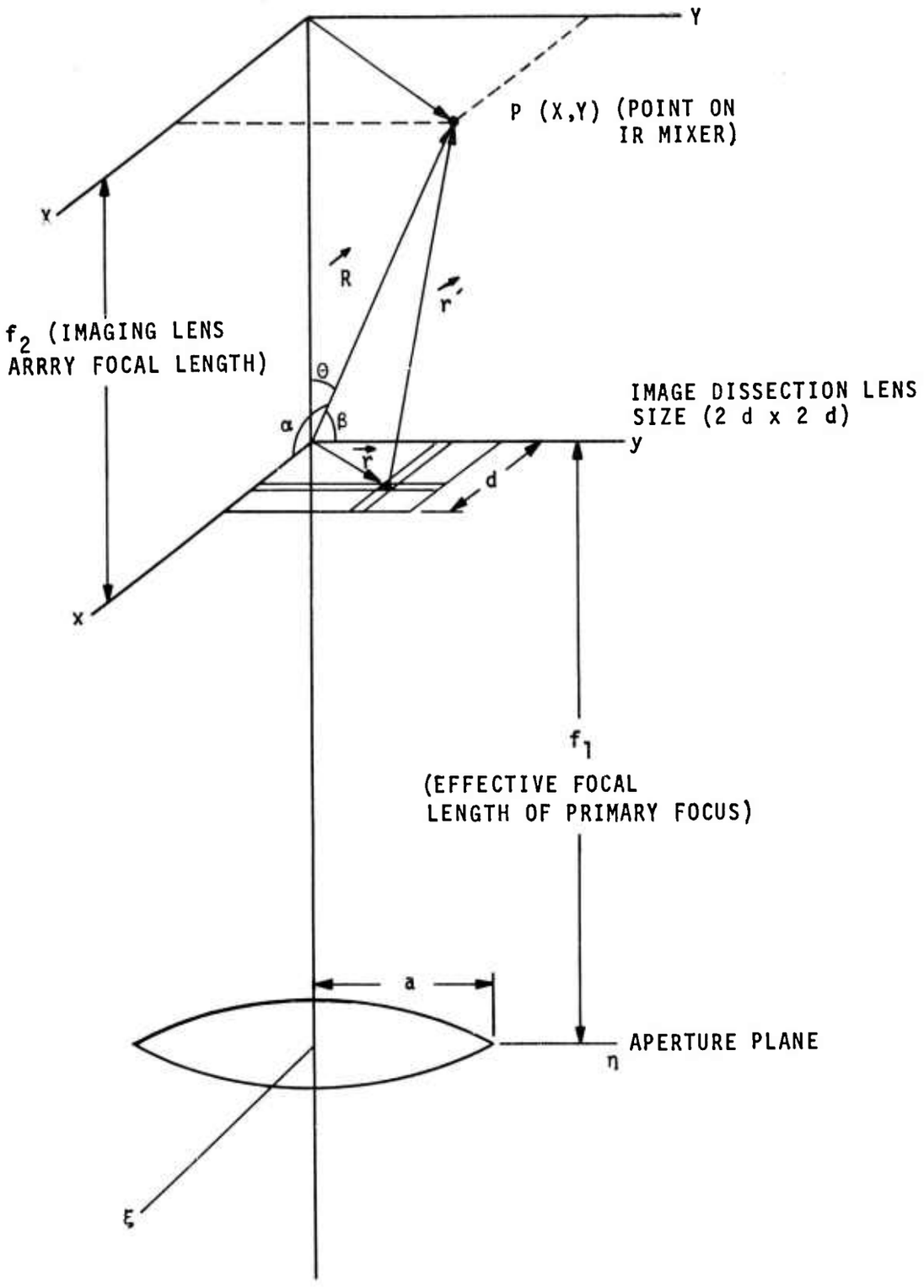

FIGURE 37. COORDINATE FOR HETERODYNE RECEIVER BEAM PATTERN ANALYSIS

The diffraction pattern formed in the focal plane of the image-dissection array due to the diffraction field incident upon the array can then be found from reference 11 as:

$$\overline{E}p_s(X, Y) = \int_{-d}^{d} \int_{-d}^{d} I_o(x, y)\, e^{ik(\alpha x + \beta y)}\, dxdy \qquad (2)$$

Substituting for I_o in equation 2 and making a small angle approximation,

$$X = R\alpha = f_{2\alpha}$$

$$Y = R\beta = f_{2\beta}$$

we get:

$$\overline{E}p_s(X, Y) = 2\pi a^2 \int_{-d}^{d} \int_{-d}^{d} \frac{J_1\left\{\frac{ka}{f_1}\left[(x + x')^2 + (y + y')^2\right]^{1/2}\right\}}{\frac{ka}{f_1}\left[(x + x')^2 (y + y')^2\right]^{1/2}} \cdot e^{i\frac{k}{f_2}(Xx + Yy)}\, dxdy \qquad (3)$$

where the integration is over that part of the $J_1(x)/x$ diffraction pattern that is incident upon the area of a particular image-dissection lens.

Consider now the LO similarly focused by the image-dissection lens array and we get:

$$\overline{Ep}_{LO}(X, Y) = \int_{-d}^{d} \int_{-d}^{d} \underbrace{\frac{\sin mx}{mx} \cdot \frac{\sin my}{my}}_{\text{LO field distribution over the image-dissection lens}} \cdot e^{\frac{ik}{f_2}(Xx + Yy)} \, dxdy \qquad (4)$$

where $\overline{Ep}_{LO}(X, Y)$ is the electric field of the LO wave in the focal plane of the image dissectors. The LO was chosen to be a uniform plane wave so that $m = 0$ and $\sin mx/mx \cdot \sin my/my = 1$. Substituting these values into equation 4, we get:

$$\overline{Ep}_{LO}(X, Y) = \int_{-d}^{d} \int_{-d}^{d} e^{\frac{ik}{f_2}(Xx + Yy)} \, dxdy \qquad (5)$$

The time dependent forms of the signal and local oscillator fields can now be written as:

$$\overline{Ep}_s(X, Y, t) = C \; e^{-i(\omega t + kf_1)} \, \overline{Ep}_s(X, Y)$$

and (6)

$$\overline{Ep}_{LO}(X, Y, t) = B \; e^{-i \omega_o t} \, \overline{Ep}_{LO}(X, Y)$$

where ω and ω_o are the frequencies of the signal and LO waves, respectively.

The fields of the received signal and the LO are now combined at the mixer by addition (assuming the polarization of the two components are aligned) and the intensity of the resultant computed.

$$I_i = < \left(E_{LO} + E_p \right)^2 > = \frac{1}{2T} \int_{-T}^{T} \left(E_{LO}^2 + E_p^2 + E_{LO} E_p^* + E_{LO}^* E_p \right) dt \tag{7}$$

The period of integration (2T) is taken very long compared to the period of the infrared frequency, but short compared to the period of the frequency difference introduced by the two cross terms. Therefore, the first two terms in the intergrand result in dc outputs from the mixer and are of no interest at this point. The two cross terms result in the intermediate IF signal. The mixer responds to the integrated intensity of the real part of the last two terms over its surface so that the mixer output is given by:

$$I_m = C' \left[\sin (\omega - \omega_o) t + kf_1 \right] \iint_{\substack{\text{mixer} \\ \text{area}}} (\text{Re})\, Ep_s(X, Y) \cdot Ep_{LO}(X, Y) \cdot dXdY$$

$$I_m = C'' \left\{ \sin \left[(\omega - \omega_o) t + kf_1 \right] \right\} \iint \frac{J_1 \left\{ \frac{ka}{f_1} \left[(x + x')^2 + (y + y')^2 \right]^{1/2} \right\}}{\frac{ka}{f_1} \left[(x + x')^2 + (y + y')^2 \right]^{1/2}} \cdot e^{\frac{ik}{f_2}(Xx + Yy)} \, dxdy \tag{8}$$

In equation 8, the argument of the sine term is made up of two parts. The first part is the time varying component that produces the IF signal. The second part is a fixed phase that can be dropped with no loss of generality.

APPENDIX C

REFERENCES

1. Arams, F. R., Sard, E. W., Peyton, B. J., and Pace, F. P., "Infrared Heterodyne Detection with Gigahertz IF Capability," IEEE Journal of Quantum Electronics, Vol QE-3, No. 11, p 484, November 1967.

2. B. J. Peyton, A. J. DiNardo, G. M. Kanischak, F. R. Arams, R. A. Lange, and E. W. Sard, "High-Sensitivity Receiver for Infrared Laser Communications," IEEE J. Quantum Electronics, Vol QE-8, No. 2, p 252-263, February 1972.

3. F. Pace, R. Lange, F. Arams, B. Peyton, and E. Sard, "Advanced Capability Infrared Receiver System," Final Report, AIL Report 3481-F, March 1970.

4. Patterson, R. J., "A GeSbSe Infrared Transmitting Glass," Proceedings of IRIS, Vol II, No. 1, October 1966.

5. d'Auria, L., Huignard, J. P., Roy, A. M., and Spitz, E., "Photolithographic Fabrication of Thin Film Lenses," Optics Communications, Vol 5, No. 4, p 232, July 1972.

6. Ramsey, John F., "Free Space Power Transmission."

7. Buczek, C. and Picus, G. S., "Applied Physics Letters 11," p 125, 1967.

8. Peyton, B., DiNardo, A., Kanischak, G., Arams, F., Lange, R., and Sard, E., "High-Sensitivity Receiver for Infrared Laser Communications," IEEE J. Quantum Electronics, Vol QE-8, No. 2, p 252-262, February 1972.

9. Vérié, C. and Sirieix, M., "Gigahertz Cutoff Frequency Capabilities of CdHgTe Photovoltaic Detectors at 10.6 μ," IEEE J. Quantum Electronics, Vol QE-8, No. 2, p 180-184, February 1972.

10. Pace, F., Arams, F., Lange, R., Peyton, B., Sard, E., and Ramsey, J., "Advanced Capability Infrared Receiver System," First Semiannual Progress Report, AIL Report 3481-I-1, October 1968.

11. Stroke, G., An Introduction to Coherent Optics and Holography, Academic Press, New York, p 22, 1966.